

Multidimensional Modeling of Internal Combustion Engine Processes

By

Vishal S. Soni

09MMET18



DEPARTMENT OF MECHANICAL ENGINEERING

AHMEDABAD-382481

May-2011

Multidimensional Modeling of Internal Combustion Engine Processes

Major Project

Submitted in partial fulfillment of the requirements

For the degree of

Master of Technology in Mechanical Engineering

(Thermal Engineering)

By

Vishal S. Soni

09MMET18



DEPARTMENT OF MECHANICAL ENGINEERING

AHMEDABAD-382481

May-2011

Declaration

This is to certify that

1. The thesis comprises original work towards the degree of Master of Technology in Mechanical Engineering (Thermal Engineering) at Nirma University and has not been submitted elsewhere for a degree.
2. Due acknowledgement has been made in the text to all other material used.

Vishal S. Soni

Certificate

This is to certify that the Major Project entitled “ Multidimensional Modeling of Internal Combustion Engine Processes ” submitted by Vishal S. Soni (09MMET18), towards the partial fulfillment of the requirements for the degree of Master of Technology in Mechanical Engineering (Thermal Engineering) of Institute of Technology of Nirma University, Ahmedabad is the record of work carried out by him under my supervision and guidance. In my opinion, the submitted work has reached a level required for being accepted for examination. The results embodied in this major project, to the best of my knowledge, haven't been submitted to any other university or institution for award of any degree or diploma.

Prof. N. K. Shah
Guide, Asst. Professor,
Department of Mechanical Engineering,
Institute of Technology,
Nirma University, Ahmedabad

Prof. V R Iyer
Professor, Head,
Department of Mechanical Engineering,
Institute of Technology,
Nirma University, Ahmedabad

Dr K Kotecha
Director,
Institute of Technology,
Nirma University, Ahmedabad

Abstract

A 2D simulation of an engine was carried out for flat piston, flat cylinder head and hemispherical cylinder head. The report reviews the Multidimensional modeling of an internal combustion engine with flat piston and flat cylinder head. This report represents the literature review for the topic and different models were considered. The modeling of the geometry have been done in Gambit 2.2 and CFD based simulation have been done in Fluent 6.2. Geometries with flat and hemispherical cylinder head is taken into account for simulation. The engine is considered in motored condition in case 1 to 7 and case 9 . In case 8 and Case 10 , modeling of engine have been done with premixed combustion. The standard $k-\varepsilon$ model is used for modeling the turbulence. The spark ignition model and premixed combustion model is used for premixed combustion modeling. The result shows the effect of engine speed on turbulence kinetic energy and analysis of premixed combustion modeling with spark ignition model. Results indicates that in suction process the high turbulence is set in due to the shear layer in the high velocity jet entering the engine cylinder. The turbulence fluctuation increase and approximately go with the high piston speed and valve lift. There will be fall in turbulence with the closure of inlet valve. During the compression process, turbulence suddenly decreases due to wall interactions.

Acknowledgements

I here by take the opportunity to express my deep sense of gratitude to my respected guide, Prof. N.K. Shah, Asst. Professor, Department of Mechanical Engineering, Institute of Technology, Nirma University, Ahmadabad, for his valuable, precious guidance and active support during the project. I am heartily thankful to him for his time to time suggestion and the clarity of the concepts of the topic that help me a lot during the study. I am very thankful to Prof. V R Iyer (Head, Department of Mechanical Engineering, Nirma University) and Dr K Kotecha (Director, Institute of Technology, Nirma University) for his kind support in all respects.

I would also like to thank my parents, and all my friends who are always beside me.

Last but not the least; we would to thank the Almighty who gave us the physical and mental strength to perform the required things in the right direction.

Vishal S. Soni

09MMET18

Contents

| | |
|---|------------|
| Declaration | iii |
| Certificate | iv |
| Abstract | v |
| Acknowledgements | vi |
| List of Figures | x |
| List of Tables | xii |
| 1 Introduction | 1 |
| 1.1 Motivation | 1 |
| 1.2 Thermodynamic model | 2 |
| 1.3 Multidimensional modeling | 3 |
| 1.4 Objectives of the project | 3 |
| 1.5 Problem Definition | 4 |
| 2 Literature Review | 5 |
| 2.1 Turbulence modeling | 5 |
| 2.1.1 Standard k- ϵ model | 7 |
| 2.2 Modeling of premixed combustion | 8 |
| 2.2.1 Laminar premixed flames | 9 |

| | | |
|----------|--|-----------|
| 2.3 | International status | 10 |
| 3 | Computational Fluid Dynamics - An Introduction | 15 |
| 3.1 | Need of CFD | 16 |
| 3.2 | Concept of CFD | 17 |
| 3.3 | Steps to solve the problems using CFD approach | 19 |
| 3.3.1 | Creation of mathematical model | 19 |
| 3.3.2 | Choose a discretization method | 19 |
| 3.3.3 | Numerical grid generation | 20 |
| 3.3.4 | Finite approximation | 22 |
| 3.3.5 | Solution of algebraic equations | 22 |
| 3.3.6 | Convergence Criteria | 23 |
| 3.4 | Discretization methods | 23 |
| 3.4.1 | Finite difference method (FDM) | 23 |
| 3.4.2 | Finite volume method (FVM) | 25 |
| 3.4.3 | Finite element method (FEM) | 26 |
| 3.5 | Mathematical models | 27 |
| 3.5.1 | Turbulence models | 27 |
| 3.5.1.1 | Choosing a turbulence model | 28 |
| 3.5.2 | Discretization | 29 |
| 3.5.2.1 | Under-relaxation | 30 |
| 3.5.3 | Convergence Criteria | 30 |
| 4 | Selection of Numerical Approach | 32 |
| 4.1 | Numerical Scheme | 32 |
| 4.2 | Equations solved by the solver | 32 |
| 4.3 | Discretization scheme | 33 |
| 4.4 | Viscous model | 33 |
| 4.5 | Dynamic mesh strategy | 33 |

| | |
|---|-----------|
| <i>CONTENTS</i> | ix |
| 4.6 Sliding mesh strategy | 35 |
| 4.7 Boundary conditions | 35 |
| 4.8 Initial conditions | 36 |
| 5 Result and Discussion | 37 |
| 5.1 Modeling and analysis of different simulation cases with 2D | 37 |
| 5.1.1 2D simulations | 38 |
| 5.2 Grid independence | 42 |
| 5.3 Vector plots and pathlines | 44 |
| 5.4 Effect of engine speed | 54 |
| 5.5 Premixed combustion model and spark ignition model analysis | 55 |
| 6 Conclusion and Scope of Future work | 61 |
| 6.1 Conclusion | 61 |
| 6.2 Scope for future work | 62 |
| Bibliography | 63 |

List of Figures

| | | |
|-----|--|----|
| 2.1 | Structure of laminar plane premixed flame | 9 |
| 3.1 | Flow around a car | 15 |
| 3.2 | The "three dimensions" of fluid dynamics | 16 |
| 3.3 | Example of structured Multiblock mesh using point to point connection | 20 |
| 3.4 | Example of unstructured mesh consisting of tringular and tetrahedral elements | 21 |
| 3.5 | Examble of quasi-structured prismatic mesh | 22 |
| 3.6 | 1D (above) and 2D (below) cartesian grid for FDM (full symbols de- note boundary nodes and open symbols denote computational nodes) [11] | 24 |
| 3.7 | A typical control volume and the notation used for a cartesian 2D grid in FVM [11] | 26 |
| 5.1 | computation Grid with different zones for case 1 to case 3 | 39 |
| 5.2 | computation domain with different zones for case 4 to case 8 | 40 |
| 5.3 | computation domain with different zones for case 9 & 10 | 40 |
| 5.4 | Volume average turbulent kinetic energy versus crank angle for cases 1, 2 and 3, with 1 degree crank angle | 43 |
| 5.5 | Vector plot of velocity at 30 crank angle for case 1 with 2D simulaltion | 45 |
| 5.6 | Vector plot of velocity at 60 crank angle for case 1 with 2D simulaltion | 45 |
| 5.7 | Vector plot of velocity at 90 crank angle for case 1 with 2D simulaltion | 46 |

| | | |
|------|---|----|
| 5.8 | Vector plot of velocity at 120 crank angle for case 1 with 2D simulaltion | 46 |
| 5.9 | Vector plot of velocity at 150 crank angle for case 1 with 2D simulaltion | 47 |
| 5.10 | Vector plot of velocity at 180 crank angle for case 1 with 2D simulaltion | 47 |
| 5.11 | Vector plot of velocity at 210 crank angle for case 1 with 2D simulaltion | 48 |
| 5.12 | Vector plot of velocity at 240 crank angle for case 1 with 2D simulaltion | 48 |
| 5.13 | Vector plot of velocity at 270 crank angle for case 1 with 2D simulaltion | 49 |
| 5.14 | Vector plot of velocity at 300 crank angle for case 1 with 2D simulaltion | 49 |
| 5.15 | Vector plot of velocity at 330 crank angle for case 1 with 2D simulaltion | 50 |
| 5.16 | Vector plot of velocity at 360 crank angle for case 1 with 2D simulaltion | 50 |
| 5.17 | Pathlines of turbulence kinetic energy at 690 crank angle for case 9 with 2D simulaltion | 51 |
| 5.18 | Pathlines of turbulence kinetic energy at 90 crank angle for case 10 with 2D simulaltion | 52 |
| 5.19 | Vector plot of velocity at 360 crank angle for case 10 with 2D simulaltion | 52 |
| 5.20 | Vector plot of velocity at 690 crank angle for case 10 with 2D simulaltion | 53 |
| 5.21 | Pathlines of turbulence kinetic energy at 690 crank angle for case 10 with 2D simulaltion | 53 |
| 5.22 | Volume average turbulent kinetic energy versus crank angle for various engine speeds for cases 4 to 7 with 2D simulations. | 54 |
| 5.23 | Volume average static pressure versus crank angle for various engine speeds for cases 4 to 7 with 2D simulations. | 55 |
| 5.24 | Volume average static temperature versus crank angle for cases 8 . . . | 56 |
| 5.25 | Contours of static temperature at 360 crank angle for case 8 | 57 |
| 5.26 | Volume average static temperature versus crank angle for cases 10 . . . | 58 |
| 5.27 | Contours of static temperature at 360 crank angle for case 10 | 59 |
| 5.28 | Volume average progressive variable versus crank angle for cases 8 & 10 | 59 |

List of Tables

| | | |
|-----|--|----|
| 5.1 | Dimension of engine for flat head and flat piston geometry | 41 |
| 5.2 | Dimension of engine for hemispherical and flat piston head geometry | 41 |
| 5.3 | Under relaxation factors | 42 |
| 5.4 | Convergence criteria | 42 |
| 5.5 | Spark model parameters for case 8 | 56 |
| 5.6 | Spark model parameters for case 10 | 57 |

Chapter 1

Introduction

1.1 Motivation

The internal combustion engines date back to 1876 when Nicolaus A. Otto discovered the first spark-ignition engine and 1892 when Rudolf Diesel developed the compression-ignition engine. Since then many research have focused on the combustion process. In present era, the main objectives of internal combustion engine researchers are to achieve the two goals of best performance and lowest possible emission levels. The quality of human comfort is improved due to present internal combustion engines. The internal combustion engines pushed the human transportation system years ahead. The lack of oil resources and increasing oil demand makes the necessity to develop the improved and efficient engines with less pollution. The improvement in engines has been achieved by different conventional methods but because of further development in computation faculties provides new methods for designing internal combustion engines.

For improved designs of engine, one need to study that what actually happing inside the engine. In engine design, complex fluid dynamics and thermo chemical interactions takes place inside the combustion chamber which plays the important role in determining efficiency and emission released. Modifying the combustion chamber is one method to increase the efficiency and reduce the pollution. For this, the better understanding of fluid dynamics inside the cylinder becomes very important. To analyze the engine performance, models with varying complexibility ranging from zero

dimensional models to multidimensional models are available. Now many software have been developed to solve these models to understand the phenomenon inside engine cylinder.

In last decades, several researches have been focused on in-cylinder fluid motion and its effect on overall engine performance. The fluid motion inside the cylinder is very complex and turbulent in nature which depend on many engine variables like combustion chamber design, swirl, squish, tumble, engine speed, intake system geometry, load on engine, valve lift and compression ratio. This non-stationary turbulence is subjected to flow recirculation and boundary layer separation. By both experiments and modern numerical techniques, one can determine the turbulence inside the engine cylinder. The experimental determination of turbulence inside the cylinder is very difficult, time consuming, needs more instrumentations that's why it is very costly. Therefore modern numerical technique of numerical simulation can determine the in-cylinder flow field. These techniques are easy to adopt different variable conditions with computational facilities then experimentation.

1.2 Thermodynamic model

The thermodynamic models are based on first law of thermodynamics where time is only independent variable. These models effectively follow the changing thermodynamic and chemical state of working fluid through the engine's intake, compression, combustion expansion and exhaust processes. These models have been developed and used extensively for to predict engine operating characteristics and to define the gas state of emission calculations. It is difficult to predict the different engine variable by governing equation alone. This is why the sub models and relations are used to bridge this gap. [1]

1.3 Multidimensional modeling

Thermodynamic models are not able to consider the spacial flow variation and temporal variation in velocity, temperature and pressure. Multidimensional models consider the spatial and temporal variation of the velocity, temperature and pressure field in one, two or three dimensions [1]. Multidimensional models are based on the time dependent three-dimensional conservation equations of mass, momentum, energy and species. The principal components of these multidimensional engine flow models are the following[1]:

1. The mathematical models or equations used to describe the flow processes. Especially important is the turbulence model, which describes the small-scale features of the flow which are not accessible to direct calculation.
2. The Discretization procedures used to transform the differential equations of the mathematical model into algebraic relations between discrete values of velocity, pressure, temperature, etc., located on a computing mesh which (ideally) conforms to the geometry of the combustion chamber with its moving valves and piston.
3. The solution algorithm whose function is to solve the algebraic equations.
4. The computer codes which translate the numerical algorithm into computer language and also provide easy interfaces for the input and output of information

1.4 Objectives of the project

To simulate of a reciprocating engine including all processes i.e.suction, compression, expansion, and exhaust for flat cylinder head & hemispherical cylinder head & flat piston with one valve and one port , both the valves & with and without combustion in 2D.

1.5 Problem Definition

The geometric model used for the simulation is a two valve engine cylinder with its intake and exhaust manifolds. The inlet manifold downstream of the carburetor is taken into account. The simulation of engine's intake, compression, expansion and exhaust processes have to done without & with combustion for engine's parametric and design characteristic analysis. The flat piston and flat cylinder head is considered at initial state and then hemispherical cylinder head analysis is also included.

Chapter 2

Literature Review

Turbulence is the important phenomenon in the performance analysis of spark ignition engines, in recent times there is tremendous interest in the literature in the determining the turbulence parameters. A number of papers published by different researchers are reviewed in this work.

2.1 Turbulence modeling

The flow field inside an internal combustion engine is turbulent in nature and this contains many time and length scale. Such turbulent flow is depends on fluctuating velocity field. These fluctuations mix transported quantities such as momentum, energy and species concentration and cause the transported quantities to fluctuate as well. Since these fluctuations may be in small scale and frequency, but they are computationally very expensive to simulate practical engineering problems. The instantaneous governing equation can be assumed time averaged to remove the small scale, this results in a modified set of equations which are less expensive to solve. However these modified set of equations contains some additional set of unknown variables[2]. To determine these additional unknown variable in terms of known quantities, turbulence models are required.

Considering time average, one can decompose the flow variables into the sum of mean and fluctuating component as:

$$\phi = (\phi) + \phi' \quad (2.1)$$

where

$$(\phi') = 0$$

and

$$(\phi) = \lim_{\tau \rightarrow \infty} \int_t^{t+x} \phi dt \quad (2.2)$$

Where ϕ is any of the flow variables.

Therefore continuity equation is

$$\frac{\partial \rho}{\partial t} + \frac{\partial \bar{u}_i}{\partial x_j} = 0 \quad (2.3)$$

The momentum in the x, y, and z direction are:

$$\rho \left[\frac{\partial \bar{u}}{\partial t} + \bar{u} \frac{\partial \bar{u}}{\partial x} + \bar{v} \frac{\partial \bar{u}}{\partial y} + \bar{w} \frac{\partial \bar{u}}{\partial z} \right] = -\frac{\partial \bar{p}}{\partial x} + \mu \nabla^2 \bar{u} - \rho \left[\frac{\partial \bar{u}'^2}{\partial x} + \frac{\partial \bar{u}'v'}{\partial y} + \frac{\partial \bar{u}'w'}{\partial z} \right] \quad (2.4)$$

$$\rho \left[\frac{\partial \bar{v}}{\partial t} + \bar{u} \frac{\partial \bar{v}}{\partial x} + \bar{v} \frac{\partial \bar{v}}{\partial y} + \bar{w} \frac{\partial \bar{v}}{\partial z} \right] = -\frac{\partial \bar{p}}{\partial y} + \mu \nabla^2 \bar{v} - \rho \left[\frac{\partial \bar{u}'v'}{\partial x} + \frac{\partial \bar{v}'^2}{\partial y} + \frac{\partial \bar{v}'w'}{\partial z} \right] \quad (2.5)$$

$$\rho \left[\frac{\partial \bar{w}}{\partial t} + \bar{u} \frac{\partial \bar{w}}{\partial x} + \bar{v} \frac{\partial \bar{w}}{\partial y} + \bar{w} \frac{\partial \bar{w}}{\partial z} \right] = -\frac{\partial \bar{p}}{\partial z} + \mu \nabla^2 \bar{w} - \rho \left[\frac{\partial \bar{u}'w'}{\partial x} + \frac{\partial \bar{v}'w'}{\partial y} + \frac{\partial \bar{w}'^2}{\partial z} \right] \quad (2.6)$$

And the three -dimensional energy equation is:

$$\left[\frac{\partial \bar{T}}{\partial t} + \bar{u} \frac{\partial \bar{T}}{\partial x} + \bar{v} \frac{\partial \bar{T}}{\partial y} + \bar{w} \frac{\partial \bar{T}}{\partial z} \right] = \frac{k}{\rho C_p} \nabla^2 \bar{T} - \rho \left[\frac{\partial \bar{u}'T'}{\partial x} + \frac{\partial \bar{v}'T'}{\partial y} + \frac{\partial \bar{w}'T'}{\partial z} \right] \quad (2.7)$$

2.1.1 Standard k- ε model

The above approach has two tasks:

1. To relates the Reynolds stress to the turbulence parameters and to the mean flow field.
2. To determine the distribution of the parameter over flow field.

Most approaches employs the eddy-viscosity concept, where in equations 2.4 to 2.6 , right hand side terms relates to eddy viscosity, velocity gradients and turbulence kinetics energy 2.8.

$$\overline{u'_i u'_j} = \nu_t \left(\frac{\partial \overline{u}_i}{\partial x_j} + \frac{\partial \overline{u}_j}{\partial x_i} \right) - \frac{2}{3} k \delta_{ij} \quad (2.8)$$

The eddy viscosity is computed from a velocity scale ($k^{\frac{1}{2}}$) and a length scale ($k^{\frac{3}{2}}/\varepsilon$) which are predicted at each point in the flow via solution of the transport equation for turbulence kinetic energy (k) and its dissipation rate (ε).

Thus the standard k- ε model is a semi-empirical model based on model transport equations for the turbulence kinetic energy (k) and its dissipation rate (ε). The model transport equation for k was derived from the exact equation, while the model transport equation for ε was obtained using physical reasoning and bears little resemblance to its mathematically exact counterpart. In the derivation of the k- ε model, it was assumed that the flow is fully turbulent, and the effects of molecular viscosity are negligible. The standard k- ε model is therefore valid only for fully turbulent flows.

The turbulent kinetic energy k and its dissipation ε are determined using the above approach and their equations can be written as:

$$\frac{\partial}{\partial t} (\rho k) + \frac{\partial (\rho k u_i)}{\partial x_i} = \frac{\partial}{\partial x_j} \left[\left(\mu + \frac{\mu_x}{\sigma_k} \right) \frac{\partial k}{\partial x_j} \right] + G_k + G_b - \rho \varepsilon - Y_m + S_k \quad (2.9)$$

$$\frac{\partial}{\partial t} (\rho \varepsilon) + \frac{\partial (\rho k \varepsilon u)}{\partial x_i} = \frac{\partial}{\partial x_i} \left[\left(\mu + \frac{\mu_x}{\sigma_\tau} \right) \frac{\partial \varepsilon}{\partial x_j} \right] + C_{1\tau} \frac{\varepsilon}{k} (G_k + C_{3\tau} G_b) - C_{2\tau} \rho \frac{\varepsilon^2}{k} + S_\tau \quad (2.10)$$

In these equations, represent the generation of turbulence kinetic energy due to the mean velocity gradients, G_b is the generation of turbulence kinetic energy due to buoyancy; Y_M represents the contribution of the fluctuating dilation in compressible turbulence to the overall dissipation rate; $C_{1\tau}, C_{2\tau}$ and $C_{3\tau}$ are constants; σ_k and σ_τ are turbulent Prandtl for k and ε , respectively. S_k and S_τ are user defined source terms.

The turbulent (or eddy) viscosity, μ_t , is computed by combining k and ε as follows:

$$\mu_t = \rho C_\mu \frac{k^2}{\varepsilon} \quad (2.11)$$

where C_μ is a constant.

2.2 Modeling of premixed combustion

In premixed combustion the fuel and air is mixed prior to combustion. The equivalence ratio may be define as the strength of mixture. During the combustion in a premixed flame, the flame front propagates with a certain speed and the burnt products remains behind the flame front. In premixed combustion, laminar and turbulent flame speeds and reaction progress variable are used to formulate models[3]. If T_u is temperature of unburnt gas, T_b is temperature of burnt gas and T is flame temperature, then the reaction progress variable is defined as given below,

$$c = \frac{T - T_u}{T_b - T_u} \quad (2.12)$$

The reaction progress variable can also be defined as,

$$c = \frac{Y_F - Y_F^u}{Y_F^b - Y_F^u} \quad (2.13)$$

where Y_F , Y_F^u and Y_F^b are local, unburnt and burnt fuel mass fractions, respectively. For unburnt mixture the value of reaction progress variable is zero and unity for burnt mixture.

In premixed combustion, the reaction progress variable c is governed by the following transport equation,

$$\frac{\partial}{\partial t}\rho c + \frac{\partial}{\partial x_i}\rho u_i c = \frac{\partial}{\partial x_i}\left(\rho D \frac{\partial c}{\partial x_i}\right) + \dot{\omega} \quad (2.14)$$

2.2.1 Laminar premixed flames

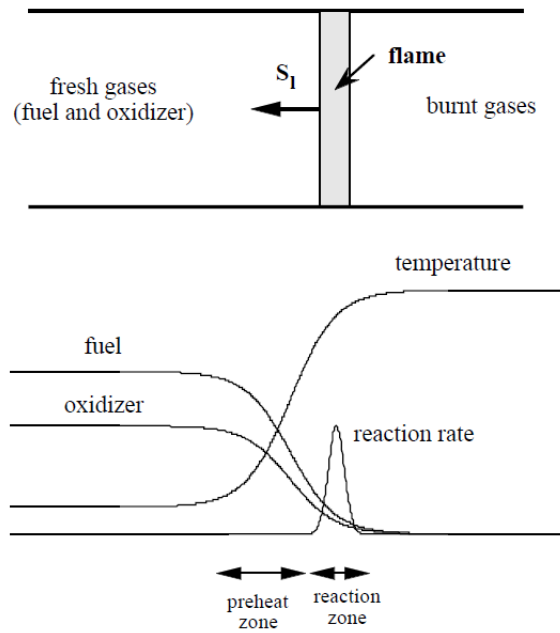


Figure 2.1: Structure of laminar plane premixed flame

The structure of a laminar premixed flame is displayed in Fig. 2.1. Fresh gases (fuel and oxidizer mixed at the molecular level) and burnt gases (combustion products) are separated by a thin reaction zone (typical thermal flame thickness, δ_L , are about 0.1 to 1 mm)[4]. Another characteristic of a premixed flame is its ability to propagate towards the fresh gases. Because of the temperature gradient and the corresponding thermal fluxes, fresh gases are preheated and then start to burn. The local imbalance between diffusion of heat and chemical consumption leads to the propagation of the front. The propagation speed S_L of a laminar flame depends on various parameters

such as fuel and oxidizer compositions, fresh gases temperature and is about 0.1 to 1 m/s. There is an interesting relation between the thermal flame thickness, δ_L , the laminar flame speed, S_L and the kinematic viscosity of the fresh gases, ν :

$$Re_f = \frac{\delta_L S_L}{\nu} \quad (2.15)$$

where Re_f is flame Reynolds number.

For a one-step irreversible simple chemical scheme:



the flame is described using a progress variable c , such as $c = 0$ in the fresh gases and $c = 1$ in the fully burnt ones. This reaction progress variable is given by equation 2.12 and equation 2.13.

For an unity Lewis number (same molecular and thermal diffusivities), without heat losses (adiabatic combustion) and compressibility effects, the two definitions are equivalent and mass and energy balance equations reduce to a single balance equation for the progress variable as given in equation 2.14.

2.3 International status

Z. Barbouchi and J. Bessrou (2009) studied the turbulent and time dependant flow inside a cylinder of an engine through investigation of distribution of the turbulent kinetic energy in whole space of chamber[5]. The study carried out during the intake stroke. They used arbitrary langaragian eulerian technique coupled with the finite element method to solve the Navier Stroke equations. They studied the variation of tumble ratio with different crank angles. The magnitude of tumble ratio increases significantly with downward motion of piston. It reached maximum at 90 CA. due to maximum engine speed it reach at maximum at 90 CA. when crank angle becomes superior at 180 CA, the tumble ratio decreases and reach for nil value for 180 CA. They also studied the effect of turbulence model into the pressure and velocity fields. They found that turbulence model of the inlet air in the cylinder has a great influence

in to the performance of the engine. It governs directly the rate of filling up, the thermal exchanges and the combustion quality. They conclude that the numerical simulation by means of finite element method with the arbitrary Lagrangian Eulerian description gives satisfied results compared to the finite volume method. As well, the study of the turbulent kinetic energy conducts to locate the maximum, the minimum and the way of variation from the cylinder symmetry axis to the lateral wall and from the air admission zone to the surface piston. Finally, the tumble ratio drawing has shown parabolic variation with crank angle interval $[0^\circ, 180^\circ]$. The peak of magnitude of tumble ratio is obtained at the centre of the mentioned interval corresponding with the maximum engine speed at this crank angle. They also indicated that the Prandtl model can be kept as the turbulence model in predicting the pressure and the velocity fields due to its simplicity and accurate results with regard to the $k-\varepsilon$ model.

Huang, Yang and Yeh (2008) studied the temporal and spatial evolution processes of the in-cylinder flow structures and turbulence intensities in the symmetry and offset planes of a motored four-valve, four-stroke engine during the intake and compression strokes using a particle image velocimeter (PIV)[6]. Two pistons of different crown shapes (flat-crown and slightly concave-crown pistons) were studied. A four-stroke, four-valve, dual-cylinder engine with V- 90° arrangement was used for the study. Each cylinder had a bore of 60.0 mm, stroke of 66.0 mm, and displacement of $186.6 \text{ cm}^3/\text{stroke}$. The shape of the cylinder head was hemispherical on the top of the combustion chamber. The inlet and exhaust valves were arranged on opposite sides of the central axis. The angle between the inlet and exhaust valve faces is 143° . The diameters of the inlet and exhaust valves were 23.2 mm and 19.8 mm, respectively. The maximum lifts of the inlet and exhaust valves was 6.8 mm and 6.6 mm, respectively. The inlet valve opens at 63° crank angle before top dead center (bTDC) and closes at 93° crank angle after bottom dead center (aBDC). The exhaust valve opens at 90° crank angles before bottom dead center (bBDC), and closes at 62° after top dead center (aTDC). The angle between the central axis of the inlet valve and the symmetry axis of the cylinder is 19° . Two piston heads with flat and slightly concave top surfaces respectively, was used for experiment. The diameter of

the piston was 59.40 mm. The compression ratios of engine with the flat-crown and concave- crown pistons were 11.0 and 10.92, respectively.

They presented the results for tumble flow motion with flat-crown piston and slightly concave-crown piston in offset and symmetric plane[6]. They plotted different graphs for evolution of tumble flow motion in symmetry plane during compression stroke at 210°, 240°, 270°, 300° CA respectively and in offset plane during intake stroke at 60°, 90°, 120°, 150°, 179° CA respectively and also the evolution of tumble flow motion in offset plane during compression stroke at 210°, 240°, 270°, 300° CA respectively for flat crowned piston. They found that the evolution processes of the large vortical flow structures in the symmetry plane of the engine cylinder installed with the slightly concave-crown piston look similar to those of the engine which is installed with the flat-crown piston.

The result shows that the flat-crown piston induces higher bulk-averaged tumble ratio and turbulence intensity than the slightly concave-crown piston does because the tumble ratio and turbulence generated by the flat-crown piston in the offset planes during the compression stroke are particularly large[6]. The engine with the flat-crown piston also presents larger torque and power outputs and lower hydrocarbon emission than that with the slightly concave-crown piston.

Kihyung Lee, Choongsik Bae and Kernyong Kang (2006), studied the effects of in- cylinder flow patterns, such as tumble and swirl flows, on combustion were experimentally investigated in a 4-valve S.I. engine[7]. Tumble flows were generated by intake ports with entry angles of 25°, 20° and 15°. Inclined tumble (swirl) flows were induced by two different swirl control valves. The initial flame propagation was visualized by an ICCD camera, the images of which were analyzed to compare the enflamed area and the displacement of initial flames. The combustion duration was also calculated by the heat release analysis. The in-cylinder flow field was measured by fiber coupled laser Doppler velocimetry (LDV) with various configurations to measure axial, swirl and radial components.

It was found that a correlation existent between the stronger tumble during induction and turbulence levels at the time of ignition results in a faster flame development[7]. As confirmed by flame propagation images and measurements of

combustion periods, tumble (swirl) was found to be more effective than pure tumble in effecting rapid and stable combustion under lean mixture conditions.

R.F. Huang, C.W. Huang, S.B. Chang, H.S. Yang, T.W. Lin and W.Y. Hsu (2005) studied the evolution processes of the in-cylinder flows in the axial and diametral planes of a motored two-valve, single cylinder, four-stroke engine during the intake and compression strokes are diagnosed by using a particle image velocimeter[8]. A device, which is called the “inlet deflection-valve”, being capable of deflecting the inlet flow is installed upstream of the inlet port. The engine cylinder, piston, and accessories were modified to meet the requirements of laser light sheet shooting and camera viewing when the particle image velocimetry is applied. A conditional sampling technique was employed to acquire the instantaneous velocity data at pre-determined crank angles. Ensemble averages of large amounts of the instantaneous velocity maps obtained at various crank angles present clear pictures of the evolution processes of the tumble and swirl motions in the engine cylinder. Sectional streamlines and the velocity vectors show the topological flow structures. The inception, establishment, evolution, and destruction processes of the swirling and tumbling vortical structures during the intake and compression strokes was studied by authors. Quantified strengths of the rotating motions in the axial and diametral planes was presented by dimensionless tumble and- swirl ratios, which was defined as the ratio of the mean angular velocity of the vortices in the target plane at a certain crank angle divided by the average crank angle velocity.

They collected data for evolution of swirl motion for different symmetry axis plane and diametral plane during different crank angles during intake and compression stroke at 1500 rpm engine speed. The velocity data was ensemble-averaged from 100 instantaneous measurements.

They found that when the inlet stream is deflected drastically, apparent swirl motion in the symmetry axial plane would be established during the intake stroke[8]. A complete swirling vortical flow structure occupying the whole diametral plane occurs at the final stage of the intake stroke. The strength of the swirl motion increases with the increase of the crank angle and attains maximum as the piston is going downward and passing halfway through the intake stroke. The strength of

the swirl motion keeps increasing during the first half of the compression stroke and decays successively.

Nureddin Dinler, and Nuri Yucel (2007) modelled an axisymmetric homogeneous charged spark ignition engine. Fluid motion and combustion process were investigated numerically[9]. Turbulent flow conditions were considered. Standard k- ϵ turbulence model for fluid flow and eddy break-up model for turbulent combustion were utilized. The effects of valve angle on the fluid flow and combustion were analyzed for constant air/fuel and compression ratios

The governing equations subject to relevant boundary conditions were solved numerically using finite-volume method. The upwind technique was employed to discretize the convective terms. A computer term had been developed by using the SIMPLE algorithm. In order to obtain a solution independent of the grid distribution, grid sensitivity tests were performed by tracing the cylinder pressure against crank angle.

They assumed that spark plug and inlet/exhaust valves are located at the centreline of cylinder[9]. Computations were performed for three different inlet valve angles, 30°, 45° and 60°, with constant engine speed $N=2400$ rpm, compression ratio was 9:1 and excess air ratio was 1.0. Cylinder radius was 0.05 m, stroke was 0.09 m. Methane (CH_4) was used as a fuel.

They found that for inlet valve angle $\alpha=30^\circ$, combustion velocity was higher than that for $\alpha=45^\circ$ and $\alpha=60^\circ$. The combustion velocity was slowest for the valve angle $\alpha=60^\circ$. However, the fuel consumption dependency was weakly related to the valve angle.

Chapter 3

Computational Fluid Dynamics - An Introduction

In automotive applications CFD is nowadays used in a large number of areas including engine components, auxiliary systems and also for modeling the aerodynamics of the car to minimise drag and optimise the down force under various operating conditions. To improve the performance of modern cars and trucks (environmental quality, fuel economy, etc.), the automobile industry has accelerated its use of high-technology research and design tools. One of these tools is CFD, whether it is the study of the external flow over the body of a vehicle, or the internal flow through the engine, CFD is helping automotive engineers to better understand the physical flow processes, and in turn to design improved vehicles. For example, Figure 3.1 shows the flow field around a family car obtained using CFD methods.

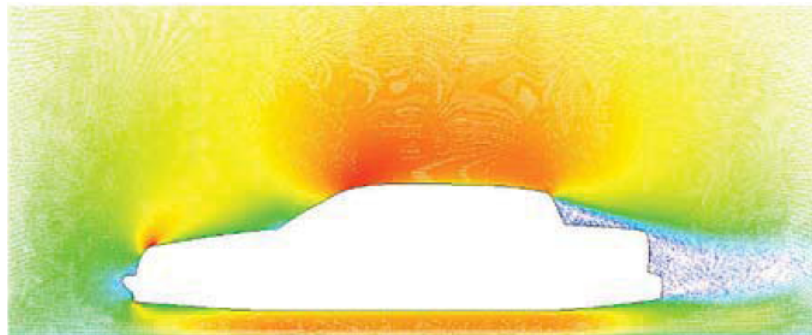


Figure 3.1: Flow around a car

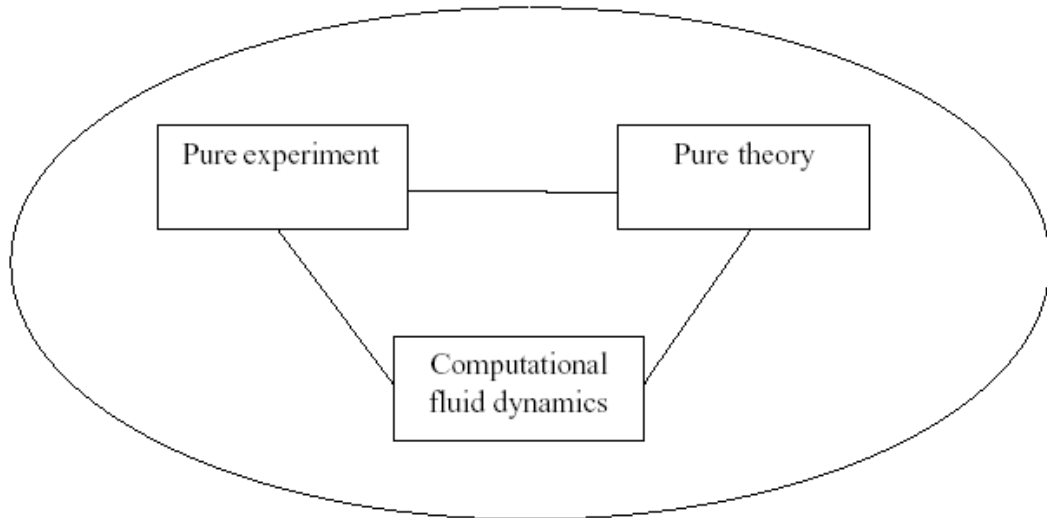


Figure 3.2: The "three dimensions" of fluid dynamics

3.1 Need of CFD

The development of the high speed computer and the evolution of the computational fluid dynamics (CFD) have a great influence on the engineering design and analysis of the Internal Combustion Engines. In the past decades, due to increasing capability to solve complex geometry and complex flow problems and reduction in computational time and costs, the CFD methodology has emerged to become an efficient approach for collecting information to improve engineering design and analysis of Internal Combustion Engines. Today, CFD is an equal partner with pure theory and pure experiment in the analysis and solution of fluid dynamics problem, as sketched in Fig.3.2. And CFD will continue to play this role indefinitely, for as long as our advanced human civilization exists.

Compared to theoretical approach to solve fluid flow problems, the CFD approach has the advantage that it can provide a solution for a much more complex problem. And compared to experimental approach, in which cost is proportional to the number of data points and the number of configurations tested, in terms of facility hire and/or man-hour costs, CFD approach can produce extremely large volumes of results at

virtually no added expense and it is very cheap to perform parametric studies, for instance to optimize equipment performance.

However, to keep things in perspective, CFD provides a new third approach- but nothing more than that. It nicely and synergistically complements the other two approaches of pure theory and pure experiment, but it will never replace either of these approaches. There will always be a need for theory and experiment. Rather, the future advancement of fluid dynamics will rest upon a proper balance of all the three approaches, with computational fluid dynamics helping to interpret and understand the results of theory and experiment, and vice versa.

3.2 Concept of CFD

The physical aspects of any fluid flow is governed by three conservation laws:

- (i) Conservation of Mass: The mass of a fluid is conserved.
- (ii) Conservation of Momentum: The rate of change of momentum is equal to the sum of the forces on a fluid particle, in the same direction (Newton's second law).
- (iii) Conservation of Energy: The rate of change of energy is equal to the sum of the rate of heat addition and the rate of work done on a fluid particle (first law of thermodynamics).

These fundamental conservation laws can be expressed in terms of basic mathematical equations, which in their most general form are either integral equations or partial differential equations. Computational fluid dynamics is the art of replacing the integrals or the partial derivatives (as the case may be) in these three fundamental equations with discretized algebraic forms, which in turn are solved to obtain numbers for the flow field values at discrete points in time and/or space. The end product of CFD is indeed a collection of numbers, in contrast to a closed-form analytical solution. However, in the long run, the objective of most engineering analyses, closed form or otherwise, is a quantitative description of the problem, i.e., numbers.

Of course, the instrument which has allowed the practical growth of CFD is the high-speed digital computer. CFD solutions generally require the repetitive manipulation of many thousands, even millions, of numbers, a task that is humanly

impossible without the aid of a computer. Therefore, advances in CFD, and its applications to problems of more and more detail and sophistication, are intimately related to advances in computer hardware, particularly in regard to storage and execution speed. This is why the strongest force driving the development of new supercomputers is coming from the CFD community. Indeed, the advancement in large mainframe computers has been phenomenal over the past three decades.[10]

Thus, in simple words CFD can be defined as:

“CFD is the analysis of systems involving fluid flow, heat transfer and associated phenomena such as chemical reactions by means of computer-based simulation.”

The technique is very powerful and spans a wide range of industrial and non-industrial application areas. Some examples are: [10]

- (i) Aerodynamics of aircraft and vehicles: lift and drag
- (ii) Turbomachinery: flows inside rotating passages, diffusers etc.
- (iii) Hydrodynamics of ships
- (iv) Marine engineering: loads on off-shore structures
- (v) Biomedical engineering: blood flows through arteries and veins
- (vi) Power plant: combustion in IC engines and gas turbines
- (vii) Chemical process engineering: mixing and separation, polymer moulding
- (viii) Electrical and electronic engineering: cooling of equipment including micro-circuits
- (ix) External and internal environment of buildings: wind loading and heating/ventilation
- (x) Environmental engineering: distribution of pollutants and effluents
- (xi) Hydrology and oceanography: flows in rivers, estuaries, oceans
- (xii) Meteorology: weather prediction

The advantages of CFD over experimental approach to fluid system design can be summarized as:

- (a) Substantial reduction of lead times and costs of new designs.
- (b) Ability to study systems where controlled experiments are difficult or impossible to perform (e.g. very large systems).
- (c) Ability to study systems under hazardous conditions at and beyond their

normal performance limits (e.g. safety studies and accident scenarios).

- (d) Practically unlimited level of detail of results. [10]

3.3 Steps to solve the problems using CFD approach

The various steps required to solve the problem using CFD are described below.[11]

3.3.1 Creation of mathematical model

The starting point of any numerical method is to convert the physical problem into the mathematical model, i.e. the set of partial differential or integral-differential equations and specify the boundary conditions. One chooses an appropriate model for the target application . This model may include simplifications of the exact conservation laws. A solution method is usually designed for a particular set of equations. Trying to produce a general purpose solution method, i.e. one which is applicable to all flows, is impractical, if not impossible and, as with most general purpose tools, they are usually not optimum for any one application.

3.3.2 Choose a discretization method

After selecting the mathematical model, one has to choose a suitable discretization method , i.e. a method of approximating the differential/integral equations by a system of algebraic equations for the variables at some set of discrete locations in space and time. There are many methods, but the most important ones are:

- (i) Finite Difference Method (FDM)
- (ii) Finite Volume Method (FVM) and
- (iii) Finite Element Method (FEM)

Other methods, like spectral schemes, boundary element methods, and cellular automata are used in CFD but their use is limited to special classes of problems. Each type of method yields the same solution if the grid is very fine. However, some

methods are more suitable to some classes of problems than others. The preference is often determined by the attitude of the developer.

3.3.3 Numerical grid generation

The discrete locations at which the variables are to be calculated are defined by the numerical grid which is essentially a discrete representation of the geometric domain on which the problem is to be solved. It divides the solution domain into a finite number of sub domains (elements, control volumes etc.) and gives the set of discrete points for the Discretization scheme.

Some of the options available are the following:

(a) Structured (regular) grid

Regular or structured grids consist of families of grid lines with the property that members of a single family do not cross each other and cross each member of the other families only once. . Although the element topology is fixed, the grid can be shaped to be body fitted through stretching and twisting of the block. Really good structured grid generators utilize sophisticated elliptic equations to automatically optimize the shape of the mesh for orthogonality and uniformity. An example of a structured Example of structured Multiblock grid is shown in Fig. 3.3

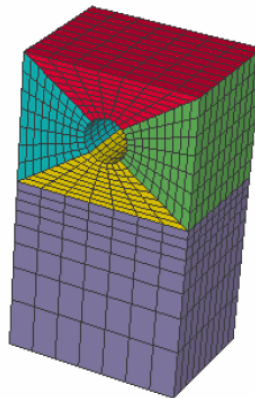


Figure 3.3: Example of structured Multiblock mesh using point to point connection

(b) Unstructured grids

For very complex geometries, the most flexible type of grid is one which can fit an arbitrary solution domain boundary. In principle, such grids could be used with any discretization scheme, but they are best adapted to the finite volume and finite element approaches. In practice, grids made of triangles or quadrilaterals in 2D, and tetrahedra or hexahedra in 3D are most often used. An example of an unstructured grid is shown in Fig. 3.4.

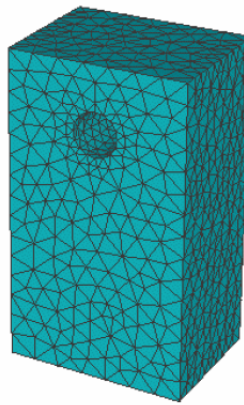


Figure 3.4: Example of unstructured mesh consisting of triangular and tetrahedral elements

(c) Hybrid grid

Hybrid grid methods are designed to take advantage of the positive aspects of both structured and unstructured grids. Hybrid grids utilize some form of structured grid in local regions while using unstructured grid in the bulk of the domain.

Hybrid grids can contain hexahedral, tetrahedral, prismatic, and pyramid elements in 3D and triangles and quadrilaterals in 2D. The various elements are used according to their strengths and weaknesses. Hexahedral elements are excellent near solid boundaries (where flow field gradients are high) and afford the user a high degree of control, but are time consuming to generate. Prismatic elements (usually triangles extruded into wedges) are useful for resolving near wall gradients, but suffer from the fact that they are difficult to cluster in the lateral direction due to the underlying triangular structure. In almost all cases, tetrahedral elements are used to

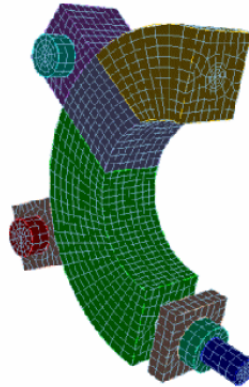


Figure 3.5: Exemple of quasi-structured prismatic mesh

fill the remaining volume. Pyramid elements are used to transition from hexahedral elements to tetrahedral elements. Many codes try to automate the generation of prismatic meshes by allowing the user to define the surface mesh and then marching off the surface to create the 3D elements. While very useful and effective for smooth shapes, the extrusion process can break down near regions of high curvature or sharp discontinuities.

3.3.4 Finite approximation

After selecting the type of grid, the next step is the finite approximations to be used in the discretization process. In a finite difference method, approximations for the derivatives at the grid points have to be selected. In a finite volume method, one has to select the methods of approximating surface and volume integrals. In a finite element method, one has to choose the shape functions (elements) and weighting functions.

3.3.5 Solution of algebraic equations

Discretization yields a large system of algebraic equations. The method of solution of these algebraic equations depends on the type of the problem i.e. steady or

unsteady. For unsteady flows, methods based on those used for initial value problems for ordinary differential equations (marching in time) are used. Steady flow problems are usually solved by pseudo-time marching or an equivalent iteration scheme. The choice of solver depends on the grid type and the number of nodes involved in each algebraic equation.

3.3.6 Convergence Criteria

Finally, one needs to set the convergence criteria for the iterative method. Usually, there are two levels of iterations: inner iterations, within which the linear equation are solved, and outer iterations, that deal with the non-linearity and coupling of the equations. Deciding when to stop the iterative process on each level is important, from both the accuracy and efficiency points of view.

3.4 Discretization methods

Basically two types of problems are there in fluid flow e.g. steady state and unsteady state. The equations of steady flow are independent of time, thus the model equation contain partial derivatives with respect to space only. But equations governing unsteady fluid flow are time dependent, thus the model equations contain partial derivatives with respect to both space and time. We can approximate these equations simultaneously and solve the resulting difference equations. The approximation can be done by any one of the following methods.

3.4.1 Finite difference method (FDM)

The first step in obtaining a numerical solution is to discretize the geometric domain i.e. a numerical grid must be defined. In finite difference method (FDM) discretization methods the grid is usually locally structured, i.e. each grid node may be considered the origin of a local coordinate system, whose axes coincide with grid

lines. This also implies that two grid lines belonging to the same family, say ξ_1 , do not intersect, and that any pair of grid lines belonging to different families, say $\xi_1 = \text{const.}$, and $\xi_2 = \text{const.}$, intersect only once. In three dimensions, three grid lines intersect at each node; none of these lines intersect each other at any other point. Fig. 3.6 shows example of one-dimensional (1D) and two-dimensional (2D) Cartesian grids used in FDM.

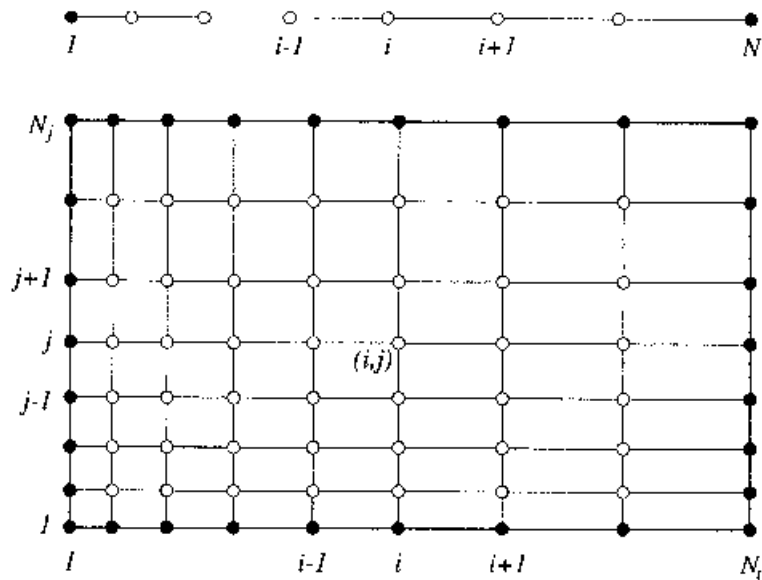


Figure 3.6: 1D (above) and 2D (below) cartesian grid for FDM (full symbols denote boundary nodes and open symbols denote computational nodes) [11]

Each node is uniquely identified by a set of indices, which are the indices of the grid lines that intersect at it, (i, j) in 2D and (i, j, k) in 3D. The neighbor nodes are defined by increasing or reducing one of the indices by unity.

Mathematical model of differential equation is given by,

$$D(\varphi) = k \tag{3.1}$$

where,

D is differential operator

k is source term

φ is parameter

In FDM the whole domain is divided into a large number of smaller elements which depends on accuracy of the solution required and derivatives are replaced by finite difference approximation. The idea behind finite difference approximations is borrowed directly from the definition of a derivative:

$$\left(\frac{\partial\phi}{\partial x}\right)_{x_i} = \lim_{\Delta x \rightarrow 0} \frac{\phi(x_i + \Delta x) - \phi(x_i)}{\Delta x} \quad (3.2)$$

Differentials can be approximated as:

$$\left(\frac{\partial\phi}{\partial x}\right)_i \approx \frac{\phi_{i+1} - \phi_i}{x_{i+1} - x_i} \quad (3.3)$$

$$\left(\frac{\partial\phi}{\partial x}\right)_i \approx \frac{\phi_i - \phi_{i-1}}{x_i - x_{i-1}} \quad (3.4)$$

$$\left(\frac{\partial\phi}{\partial x}\right)_i \approx \frac{\phi_{i+1} - \phi_{i-1}}{x_{i+1} - x_{i-1}} \quad (3.5)$$

Where, Equations 3.3, 3.4 and 3.5 are forward, backward and central differentials respectively.

Similarly for higher derivatives we have finite difference approximations. These approximations give system of algebraic equations which are then solved using computer. This is the simplest of all available approximations and easy to calculate. FDM is usually used for structured grid.[11]

3.4.2 Finite volume method (FVM)

Finite-volume methods have become popular in CFD as a result, primarily, of two advantages. First, they ensure that the discretization is conservative, i.e., mass, momentum, and energy are conserved in a discrete sense. While this property can usually be obtained using a finite-difference formulation, it is obtained naturally from a finite-volume formulation. Second, finite volume methods do not require a

coordinate transformation in order to be applied on irregular meshes. As a result, they can be applied on unstructured meshes consisting of arbitrary polyhedra in three dimensions or arbitrary polygons in two dimensions.

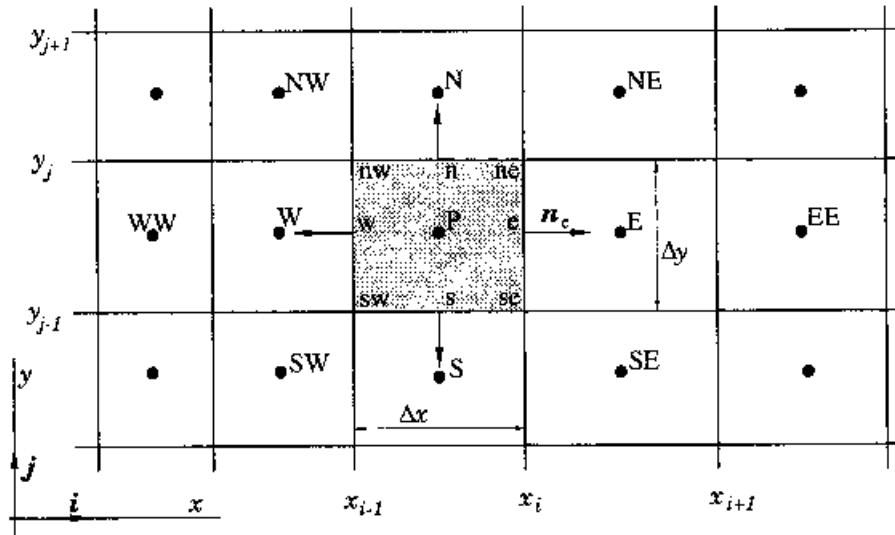


Figure 3.7: A typical control volume and the notation used for a cartesian 2D grid in FVM [11]

In FVM, the problem domain is divided into large number of small (finite) volumes. Integral forms of conservative equations are applied to each control volume. Conservation principles obey over each control volume and as well as to the entire domain. This leads to system of algebraic equations obtained for each control volume by using appropriate approximate quadrature schemes, and these equations are then solved using computer. Fig.3.7 shows a typical CV and the notation used for a cartesian 2D grid in FVM.

3.4.3 Finite element method (FEM)

This method was basically originated in the study of structural mechanics problems. It is most popular in structural mechanics and solid mechanics related fields. In general, finite element method (FEM) is versatile in applications to multidimensional complex irregular geometries. In this method, problem domain is divided into small

elements called finite elements. Using appropriate interpolation functions, approximation of function in terms of nodal values is carried out. Substitution of these approximations into governing equation (integral and differential equations) leads to system of algebraic equations, which are then solved using computer.

3.5 Mathematical models

CFD is a numerical technique to obtain an approximate solution numerically. We have to use a discretization method, which approximate the differential equations by a system of algebraic equations, which can then be solved on a computer. The approximations are applied to small domain in space and/or time so that the numerical solution provides results at discrete locations in space and/or time.

The physical aspect of any fluid flow is governed by the following three fundamental principles:

- (i) Conservation of Mass
- (ii) Conservation of Momentum
- (iii) Conservation of Energy

These fundamental principles can be expressed in terms of partial differential equations. CFD is a numerical technique to replace these partial differential equations of fluid flow into the algebraic equations by numbers and discretizing them in space and/or time domain. With the advent of high speed digital computers, CFD has become a powerful tool to predict flow characteristics in various problems in an economical way.

3.5.1 Turbulence models

Turbulent flows are characterized by fluctuating velocity fields. These fluctuations mix transported quantities such as momentum, energy, and species concentration, and cause the transported quantities to fluctuate as well. Since these fluctuations can be of small scale and high frequency, they are too computationally expensive

to simulate directly in practical engineering calculations. Instead, the instantaneous (exact) governing equations can be time-averaged, ensemble-averaged, or otherwise manipulated to remove the small scales, resulting in a modified set of equations that are computationally less expensive to solve. However, the modified equations contain additional unknown variables, and turbulence models are needed to determine these variables in terms of known quantities. There are different turbulence models available in FLUENT:

- (i) Spalart-Allmaras model
- (ii) k- ϵ models
 - Standard k- ϵ model
 - Renormalization-group (RNG) k- ϵ model
 - Realizable k- ϵ model
- (iii) k- ω models
 - Standard k- ω model
 - Shear-stress transport (SST) k- ω model
- (iv) Reynolds stress model (RSM)
- (v) Detached eddy simulation (DES) model
- (vi) Large eddy simulation (LES) model

3.5.1.1 Choosing a turbulence model

It is an unfortunate fact that no single turbulence model is universally accepted as being superior for all classes of problems. The choice of turbulence model will depend on considerations such as the physics encompassed in the flow, the established practice for a specific class of problem, the level of accuracy required, the available computational resources, and the amount of time available for the simulation. To make the most appropriate choice of model for particular application, one needs to understand the capabilities and limitations of the various options. While it is impossible to state categorically which model is best for a specific application.

3.5.2 Discretization

A control-volume-based technique is used to convert the governing equations to algebraic equations that can be solved numerically. This control volume technique consists of integrating the governing equations about each control volume, yielding discrete equations that conserve each quantity on a control-volume basis.

Discretization of the governing equations can be illustrated most easily by considering the steady-state conservation equation for transport of a scalar quantity ϕ over control volume V as follows:

$$\oint \rho \phi \vec{v} \cdot d\vec{A} = \oint \Gamma_\phi \nabla_\phi \cdot d\vec{A} + \int_V S_\phi dV \quad (3.6)$$

where,

ρ is density,

\vec{v} is velocity vector,

$d\vec{A}$ is surface area vector,

Γ_ϕ is diffusion coefficient for ϕ ,

∇_ϕ is gradient of ϕ and

S_ϕ is source of ϕ per unit volume

Above equation is applied to each control volume, or cell, in the computational domain.

Discretization of the equation on a given cell yields,

$$\sum_f^{N_{faces}} \rho_f \vec{v}_f \phi_f \cdot \vec{A}_f = \sum_f^{N_{faces}} \Gamma_\phi (\nabla_\phi)_n \cdot \vec{A}_f + S_\phi V \quad (3.7)$$

where,

N_{faces} is number of faces enclosing cell

ϕ_f is value of ϕ convected through face f

$\rho_f \vec{v}_f \cdot \phi_f$ shows mass flux through the face

\vec{A}_f is area of face f

$(\nabla_\phi)_n$ is magnitude of ∇_ϕ normal to face f

V is cell volume.

The equations solved by FLUENT take the same general form as the one given above and apply readily to multi-dimensional, unstructured meshes composed of arbitrary polyhedra. By default, FLUENT stores discrete values of the scalar ϕ at the cell centers. However, face values ϕ_f is required for the convection terms in equation 3.7 and must be interpolated from the cell center values. This is accomplished using an upwind scheme.

Upwinding means that the face value ϕ_f is derived from quantities in the cell upstream, or "upwind," relative to the direction of the normal velocity ∇_n in equation. FLUENT allows us to choose from several upwind schemes: first-order upwind, second-order upwind, power law, and QUICK. The diffusion terms in equations are central-differenced and are always second order accurate.

3.5.2.1 Under-relaxation

Because of the nonlinearity of the equation set being solved by FLUENT, it is necessary to control the change of ϕ . This is typically achieved by under-relaxation, which reduces the change of ϕ produced during each iteration. In a simple form, the new value of the variable ϕ within a cell depends upon the old value, ϕ_{old} , the computed change in ϕ , $\Delta\phi$, and the under-relaxation factor, α , as follows:

$$\phi = \phi_{old} + \alpha\Delta\phi \quad (3.8)$$

For most flows, the default under-relaxation factors do not usually require modification. If unstable or divergent behavior is observed, however, it is required to reduce the under-relaxation factors for pressure, momentum, k , and ϵ from their default values of 0.5, 0.7, 0.8 and 0.8 to about 0.2, 0.5, 0.5 and 0.5 respectively.

3.5.3 Convergence Criteria

At the end of each solver iteration, the residual sum for each of the conserved variables is computed. On a computer with infinite precision, these residuals will go to zero as the solution converges. On an actual computer, the residuals decay to some

small value (“round-off”) and then stop changing (“level out”). For “single precision” computations, residuals can drop as many as six orders of magnitude before hitting round-off whereas double precision residuals can drop up to twelve orders of magnitude. Hence, double precision solver gives more accurate results than single precision but it requires more computational time and memory.

Chapter 4

Selection of Numerical Approach

The selection of numerical approach was done as per literature survey and inherent nature of problem.

4.1 Numerical Scheme

The numerical scheme of FLUENT[®] 6.2.16 is based on the finite volume technique and involves following steps[12]:

- Integration of the governing equations of fluid flow over all the control volumes of the solution domain.
- Discretization involves substitution of the terms in the integrated equation representing flow process such as convection, diffusion and source with finite difference type approximation and thereby converting them into algebraic equations.
- Solution of the algebraic equations is obtained by an iterative method.

4.2 Equations solved by the solver

The equations which were solved by the solver were as below[12]:

- Energy
- Mass & Momentum
- Turbulence

4.3 Discretization scheme

1. Pressure Interpolation Scheme: Standard
2. Pressure–velocity coupling: SIMPLE (Semi-Implicit Method for Pressure Linked Equation) was used. The Simple Algorithm uses a relationship between velocity and pressure.
3. Momentum, Turbulent Kinetic Energy and Turbulent Dissipation rate, Energy Equation: 1st order upwind scheme was used.

4.4 Viscous model

The standard k- ϵ model was used in these simulations. The k- ϵ model is one of the most common turbulence models. It is two equation models, which mean extra transport equations to represent the turbulent modeling of flow. This allows a two equation model to account for history of effect like convection and diffusion of turbulent energy. The k-equation is a model of the transport equation for the turbulent kinetic energy, and the ϵ -equation is a model for the dissipation rate of turbulent kinetic energy. The standard k- ϵ model in FLUENT[®] falls within this class of turbulence model and has become the favorite choice of practical engineering flow calculations in the time since it was proposed by Launder and Spalding (1972). Robustness, economy, and reasonable accuracy for a wide range of turbulent flows explain its popularity in industrial flow and heat transfer simulations[12].

4.5 Dynamic mesh strategy

In an engine cylinder transient simulation is only possible with deforming computational grid. In FLUENT[®], the engine geometry is need to modeled once at a defined crank angle then further mesh modification is done by solver itself[12]. Node and

cell movement as well as the internal structure of the mesh are a result of the boundary conditions defined for the moving parts. The mesh update can be achieved by spring motion, local re-meshing, dynamic layering and a combination of these. The three possibilities can be described as follows: The spring based smoothing method addresses connections between two nodes as springs. The mesh is thus idealized as a network of interconnected springs. A displacement at a given boundary node will generate a force proportional to the displacement along the spring connected to the node. So the displacement of the boundary node is propagated through the volume mesh. At equilibrium, the net force on a node due to all the springs connected to the nodes must be zero[13]. This results in an iterative process, which is solved at each time step. The number of cells is kept constant with this method. For time being, the spring based smoothing method can be used on zones with a triangular or tetrahedral mesh. When the boundary displacement is large compared to the local cell sizes, however, the cell quality can deteriorate or the cells can become degenerate. This will lead to convergence problems when the solution is updated to the next time step. To circumvent this problem, local re-meshing is required. The solver agglomerates poor-quality cells (cells that are too large, too small, or excessively stretched) and locally re-meshes the agglomeration. The number of cells will usually change during this process. Especially for complex geometries these two methods show a flexible approach for, meshing, as a fully unstructured tetrahedral mesh, layered elements have considerable advantage for the flow and with respect to a low number of cells. A smaller cell count will reduce resource requirements and calculation time. Furthermore, a characteristic of finite volume solvers is the ability to accept much higher aspect ratios for layered elements than for tetrahedral elements. Especially in regions of small gaps like in the valve seat the solver will profit from these elements. Also layered elements tend to result in greater accuracy for regions with high gradients than tetrahedral elements do. Finally faster grid generation is performed when adding or removing layers for the next time step[12]. (FLUENT[®] User Guide, 2005)

4.6 Sliding mesh strategy

When a time-accurate solution for moving mesh is desired, the sliding mesh model is used to compute the unsteady flow field. The sliding mesh model is the most accurate method for simulating flows in multiple moving reference frames, but also the most computationally demanding. Most often, the unsteady solution that is sought in a sliding mesh simulation is time periodic. That is, the unsteady solution repeats with a period related to the speeds of the moving domains. However, we can model other types of transients, including translating sliding mesh zones.

In the sliding mesh technique two or more cell zones are used. If we generate the mesh in each zone independently, we would need to merge the mesh prior to starting the calculation. Each cell zone is bounded by at least one "interface zone" where it meets the opposing cell zone. The interface zones of adjacent cell zones are associated with one another to form a "grid interface." The two cell zones will move relative to each other along the grid interface. Note that the grid interface must be positioned so that it has fluid cells on both sides.

During the calculation, the cell zones slide relative to one another along the grid interface in discrete steps. Since the flow is inherently unsteady, a time-dependent solution procedure is required[12]. (FLUENT[®]User Guide, 2005)

4.7 Boundary conditions

The flow domain which is considered for simulation is downstream of the carburetor. Inlet valve movement is simulated using the ideal valve lift profile of the engine. The intake valve opens at TDC and the boundary condition at the inlet is assigned as pressure inlet. This inlet valve closed after 180° crank rotation at BDC and the boundary condition will changed to wall. For further 360° crank rotation the inlet valve remains close. In case 1 to 4, the exhaust valve is assumed as exhaust port instead of poppet valve and in case 5 & 10, the exhaust valve is assumed as poppet valve. After 540° of crank rotation, the exhaust port/valve opens when piston is at BDC and boundary condition will change to pressure outlet for next 180° of crank

rotation.

4.8 Initial conditions

Initial condition corresponds to a pressure of 99000 Pa for simulations. Suitable assumptions are made for remaining variable. The components of velocity are taken as 1m/s, similarly the initial value for turbulent kinetic energy is taken as $0.1\text{m}^2/\text{s}^2$ and dissipation rate as $0.1\text{m}^2/\text{s}^3$ respectively. The wall temperature is kept constant throughout the simulation as 300 k. For premixed combustion analysis the initial value of the reaction progress variable is taken zero.

Chapter 5

Result and Discussion

5.1 Modeling and analysis of different simulation cases with 2D

The 2d analysis was done in detail using FLUENT® 6.2.16 and GAMBIT 2.2.30. These cases were analyzed with inlet as a poppet valve with manifold and exhaust as a port and poppet valve for 2D. This analysis is done basically to get the variation in turbulent kinetic energy to check effect of engine speed and effect of cylinder head configurations. The analysis is carried out without and with combustion.

The model used in this are summarized below:

a) Solver

Segregated solver, unsteady state, 1st order implicit formulation, 2D space.

b) Viscous

The turbulence has been modeled using Standard k- ϵ model and the near wall treatment used was Standard Wall functions. Model constants used are as under.

$$C_{1\tau} = 1.44(\text{Equation 3.10})$$

$$C_{2\tau} = 1.92(\text{Equation 3.10})$$

$$\sigma_k = 1.00 (\text{Equation 3.9})$$

$$\sigma_\tau = 1.3 (\text{Equation 3.10})$$

$$C_\mu = 0.09 (\text{Equation 3.11})$$

c) Boundary condition

- **Intake stroke**

Inlet is defined as pressure inlet and the pressure value is assigned as 101325 Pascal and the rest of the boundary as wall.

- **Compression and Expansion Stroke**

All the boundaries are defined as wall.

- **Exhaust stroke**

Exhaust port/valve is defined as pressure outlet and the pressure value is assigned as 101325 Pascal and the rest of the boundary as wall.

d) Platform

Windows 7, Core i3 , 3 GB RAM.

5.1.1 2D simulations

Following cases with Disk head are solved and parametric study was done.

1. Flat Cylinder head, flat piston with inlet valve diameter 25 mm with Layering technique, 1500 rev/min, 1mm grid size, atmospheric pressure inlet boundary condition.

2. Flat Cylinder head, flat piston with inlet valve diameter 25 mm with Layering technique, 1500 rev/min, 2 mm grid size, atmospheric pressure inlet boundary condition.

3. Flat Cylinder head, flat piston with inlet valve diameter 25 mm with Layering technique, 1500 rev/min, 3 mm grid size, atmospheric pressure inlet boundary condition.

4. Flat Cylinder head, flat piston with inlet valve diameter 25 mm with exhaust poppet valve with Layering technique, 1500 rev/min, 1mm grid size, atmospheric pressure inlet boundary condition.

5. Flat Cylinder head, flat piston with inlet valve diameter 25 mm with exhaust poppet valve with Layering technique, 2000 rev/min, 1mm grid size, atmospheric pressure inlet boundary condition.

6. Flat Cylinder head, flat piston with inlet valve diameter 25 mm with exhaust poppet valve with Layering technique, 2500 rev/min, 1mm grid size, atmospheric pressure inlet boundary condition.

7. Flat Cylinder head, flat piston with inlet valve diameter 25 mm with exhaust poppet valve with Layering technique, 3000 rev/min, 1mm grid size, atmospheric pressure inlet boundary condition.

8. Flat Cylinder head, flat piston with inlet valve diameter 25 mm with exhaust poppet valve with Layering technique, 1500 rev/min, 1mm grid size, atmospheric pressure inlet boundary condition with premixed combustion and spark ignition model.

9. Hemispherical cylinder head, Flat piston with inlet valve diameter 30 mm with exhaust poppet valve with Layering technique, 1500 rev/min, 1mm grid size, atmospheric pressure inlet boundary condition.

10. Hemispherical cylinder head, Flat piston with inlet valve diameter 30 mm with exhaust poppet valve with Layering technique, 1500 rev/min, 1mm grid size, atmospheric pressure inlet boundary condition with premixed combustion and spark ignition model.

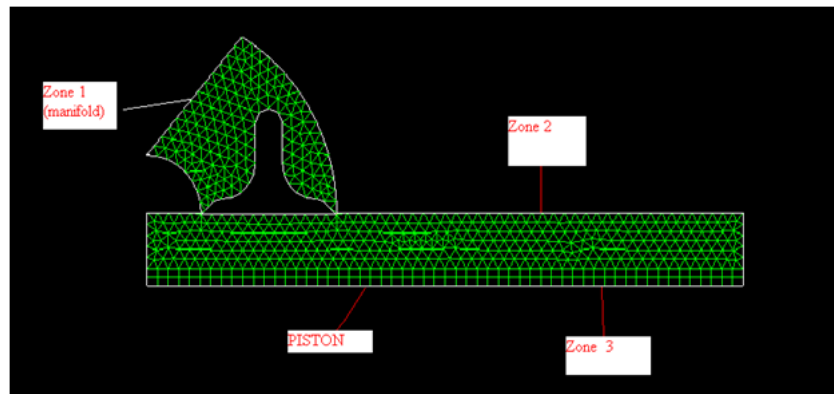


Figure 5.1: computation Grid with different zones for case 1 to case 3

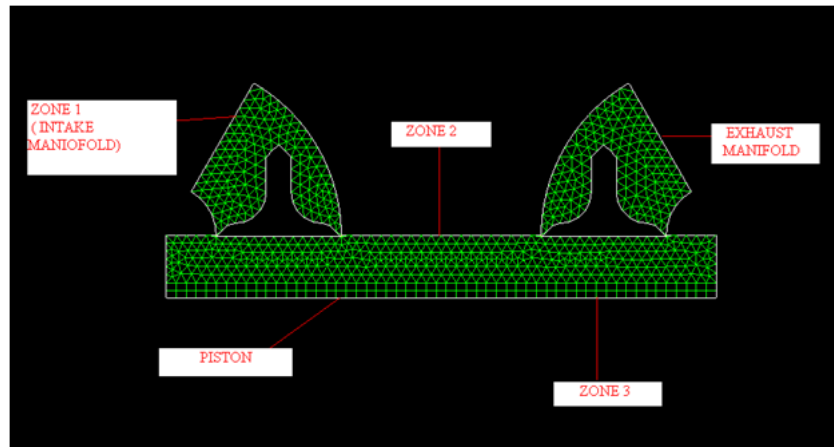


Figure 5.2: computation domain with different zones for case 4 to case 8

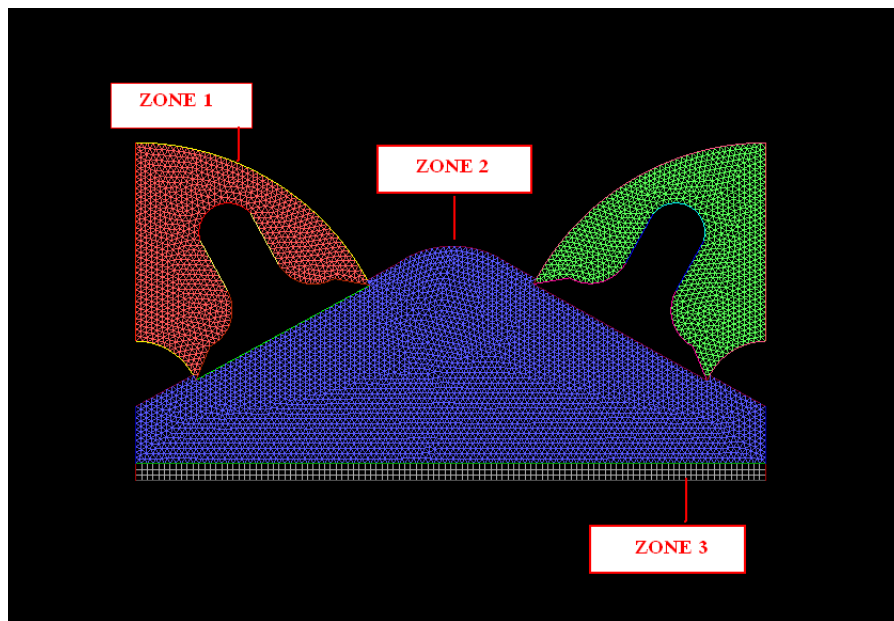


Figure 5.3: computation domain with different zones for case 9 & 10

The dimensions for different geometries are given below in table 5.1 & 5.3. Table 5.1 shows the dimension of engine geometry for cases 1 to 8 and table 5.2 shows the dimensional of engine geometry for case 9 and 10.

Table 5.1: Dimension of engine for flat head and flat piston geometry

| Parameter | size |
|------------------------------|-------------|
| Cylinder and piston diameter | 110 mm |
| Piston stroke | 100 mm |
| Connecting rod length | 110 mm |
| Compression ratio | 9 |
| Inlet valve diameter | 25 mm |
| Outlet port / valve diameter | 25 mm |
| Valve lift | 8.37 mm |

Table 5.2: Dimension of engine for hemispherical and flat piston head geometry

| Parameters | Size |
|------------------------------|-------------|
| Cylinder and piston diameter | 110 mm |
| Piston stroke | 100 mm |
| Connecting rod length | 110 mm |
| Compression ratio | 9 |
| Inlet valve diameter | 30 mm |
| Outlet port / valve diameter | 30 mm |
| Valve lift | 8.37 mm |

The computational domain used for case no. 1 to 10 are shown in Figures 5.1 to 5.3 respectively. Simple operation of vertex edges and face were used to create the cylinder geometry. For cases 1 to 3 the computational domain is divided into three zones. First zone consists of manifold, second zone consists of part of the clearance volume where valve motion takes place and the third zone consists of the remaining part of the clearance volume. The first and the second zones are meshed using Triangular type mesh, the scheme used is ‘‘Pave’’ and Re-meshing technique is applied to these zones. The third zone is meshed with quadrilateral mesh with ‘‘Map’’ scheme and layering technique is applied to this zone.

Mainly computation is done for speed of 1500 rev/min and atmospheric pressure inlet boundary condition for all models. To know effect of engine speed case 4 to 8 are simulated with speed of 1500 rev/min to 3000 rev/min in step of 500 rev/min.

For case 2 the total number of grid cells when the piston is at TDC is 1404, which increases to 3768 when it reaches at BDC. The grid interval size was of 2mm.

Computational time is around 8 hours. Under relaxation factors and convergence criteria used for solution control are as under in table 5.3 and 5.4.

Table 5.3: Under relaxation factors

| Under relaxation factors | Value |
|---------------------------------|--------------|
| Pressure | 1 |
| Density | 1 |
| Body forces | 1 |
| Momentum | 0.01 |
| Turbulent viscosity | 0.5 |
| Turbulence kinetic energy | 0.5 |
| Turbulence dissipation rate | 0.5 |
| Energy | 0.8 |

Table 5.4: Convergence criteria

| Convergence criteria | Value |
|-----------------------------|--------------|
| Continuity | 0.0001 |
| X- velocity | 0.001 |
| Y- velocity | 0.001 |
| Energy | 1e-06 |
| Turbulent kinetic energy | 1e-05 |
| Turbulent Dissipation rate | 1e-05 |

5.2 Grid independence

Figure 5.4 shows results of turbulence kinetic energy variation with different grid size. It is seen from that as grid size is decreasing turbulence kinetic energy value increases during suction and compression stroke which is indicating grid independent solution is still not achieved. But as smaller grid size is used then number of nodes increases to approximately 4 times in case of 2D . Also as piston moves from TDC to BDC more nodes will be added due to Layering technique as per grid size.

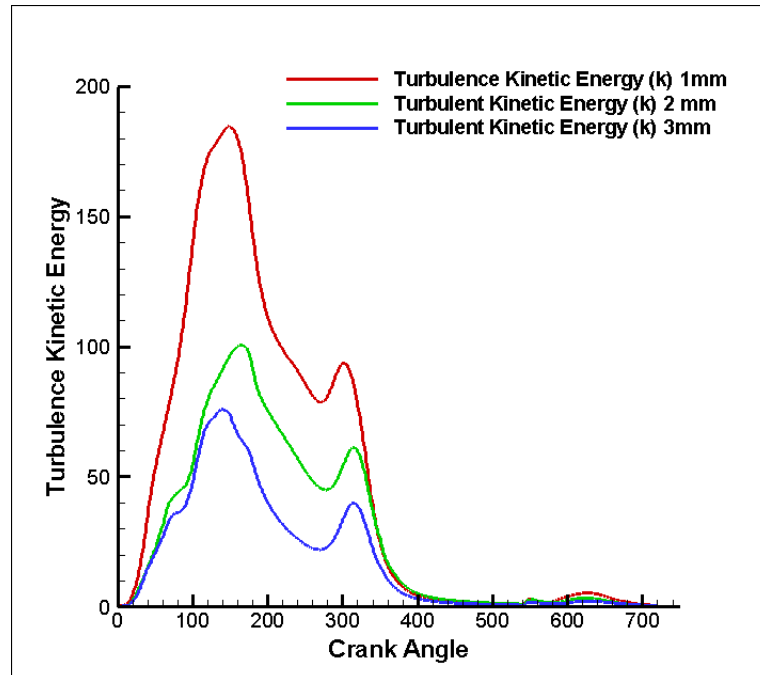


Figure 5.4: Volume average turbulent kinetic energy versus crank angle for cases 1, 2 and 3, with 1 degree crank angle

e.g For 3 mm grid size with 2D, when piston is at TDC number of cells are 483 which increases to 1621 when piston is reaching at BDC and computation time required for simulation of complete cycle is approximately 4 hours. For 2 mm grid size with 2D, when piston is at TDC number of cells are 1404 which increases to 3768 when piston reaches to BDC and computational time required for simulation of complete cycle is approximately 9 hours. For 1 mm grid size with 2D when piston is at TDC number of nodes are 3890 which increases to 15078 when piston reaches BDC and computational time required for complete simulation of cycle is approximately 15 hours. Thus, computation time will increase as we go for finer grid. Due to limitation of computation facility and time constraint, simulations with finer grid size which have grid independent solution is not possible. So practically all 2D simulations are carried out with 1 mm grid size.

Examination of the computed results from figure 5.4 reveals large variation in turbulent kinetic energy right through the induction and compression process. Initial

high turbulence is set in due to shear in the high velocity jet entering the cylinder. The turbulence fluctuation increases and approximately coincides with the point of maximum piston speed and the valve lift, further to which there is fall in turbulence kinetic energy with commencement with intake valve closure. Then during compression stroke it decays due to wall interaction and non availability of source of turbulence as in suction process. But at the end of compression process due to fluid movement in opposite direction, shear is generated which will give rise to turbulence kinetic energy and another small peak is observed. Then onwards turbulent kinetic energy decreases during expansion process. In exhaust process due to valve motion once again turbulence kinetic energy increases reaches to peak value and then decreases with closure of exhaust valve.

5.3 Vector plots and pathlines

Figure 5.16 to 5.21 shows vector plots of velocity and pathlines of turbulence kinetic energy at different crank angle. With this we can study the flow pattern of velocity inside cylinder.

Figure 5.5 to 5.16 show the vector plots of valocity magnitude in suction and compression process. This show that in suction process the high turbulence is set in due to the shear layer in the high velocity jet entering the engine cylinder. The turbulence fluctuation increase and approximately go with the high piston speed and valve lift. There will be fall in turbulence with the closure of inlet valve. During the compression process, turbulence suddenly decreases due to wall interactions. At the end of compression process the turbulence will decays and this is desirable for better combustion because the spark initiates at the end of compression stroke. If at this instant, the higher turbulence can decay the process of spark initiation which is not desirable. High turbulence during suction & compression also helps for better mixing of air fuel mixture. Figure 5.17 show that at the end of exhaust process , sufficeient turbulence ia available.

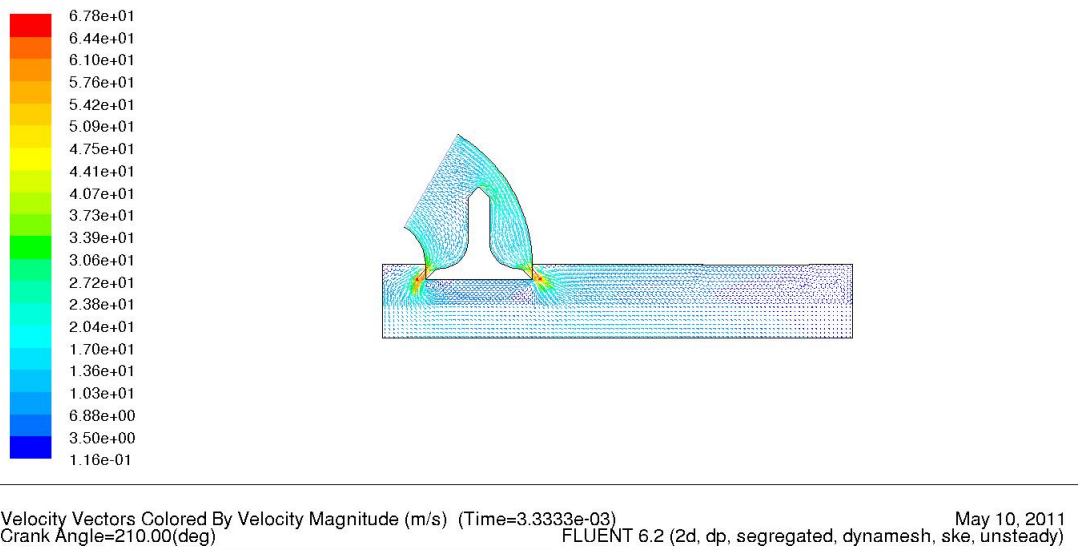


Figure 5.5: Vector plot of velocity at 30 crank angle for case 1 with 2D simulation

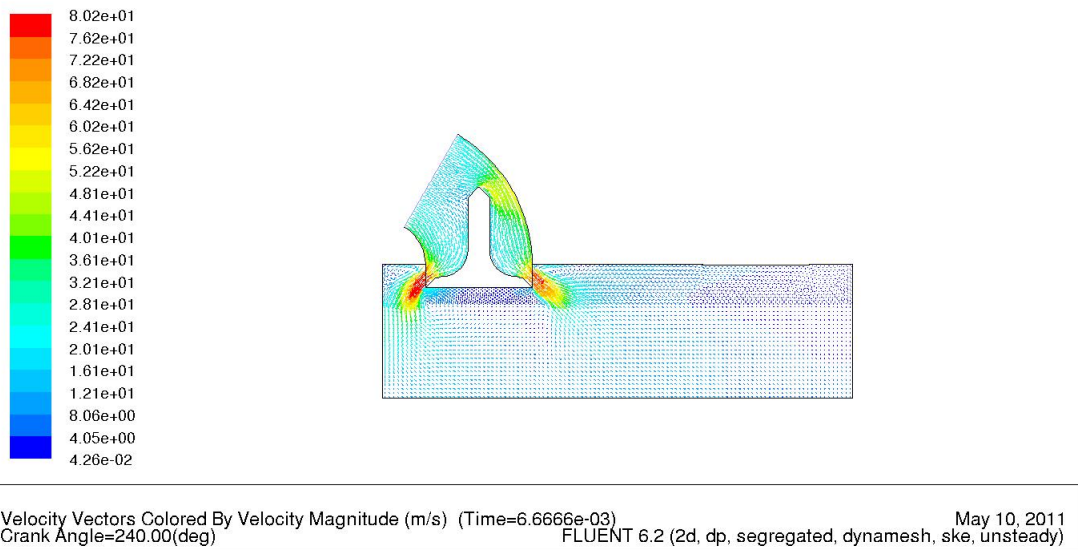


Figure 5.6: Vector plot of velocity at 60 crank angle for case 1 with 2D simulation

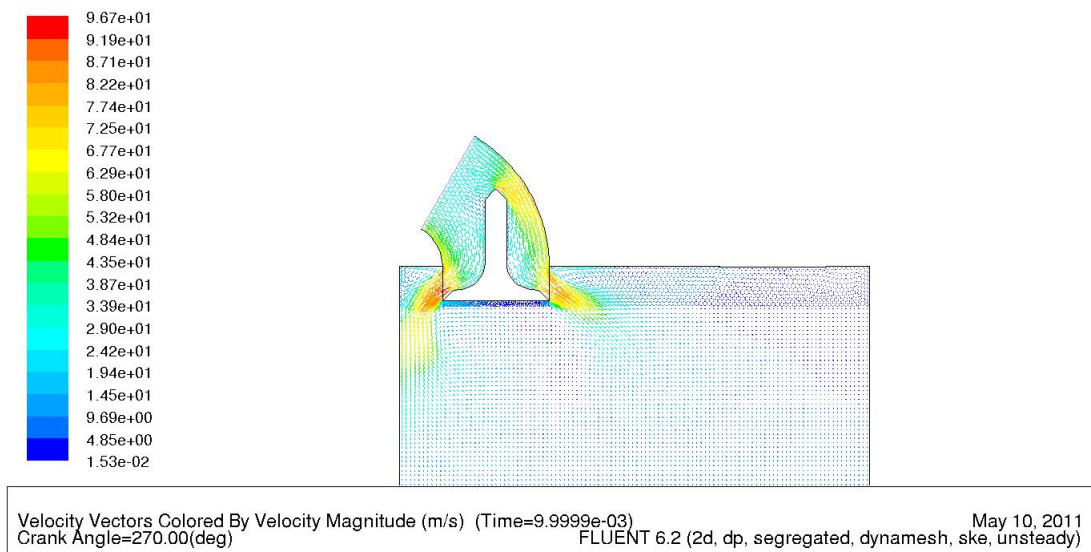


Figure 5.7: Vector plot of velocity at 90 crank angle for case 1 with 2D simulation

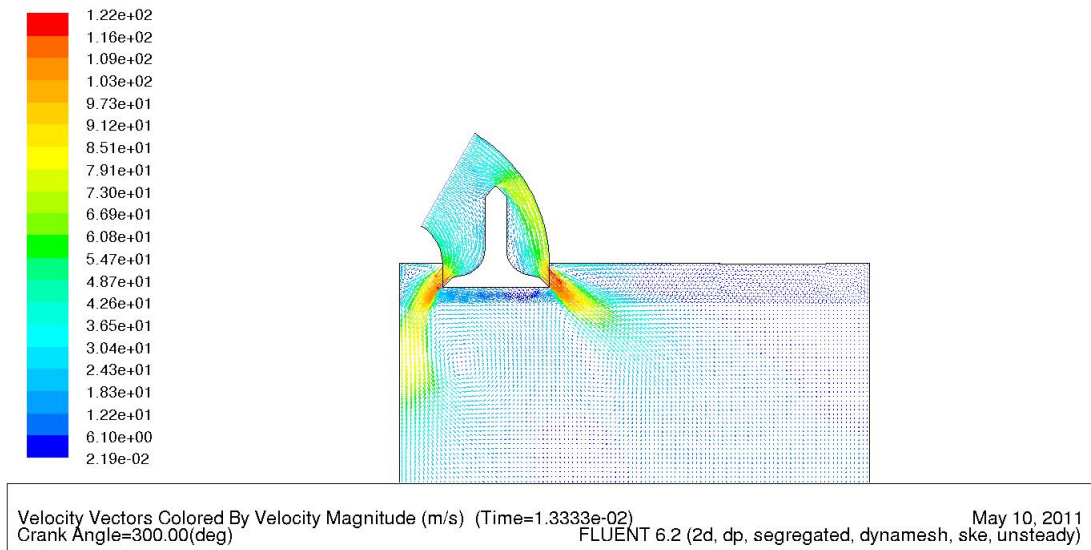


Figure 5.8: Vector plot of velocity at 120 crank angle for case 1 with 2D simulation

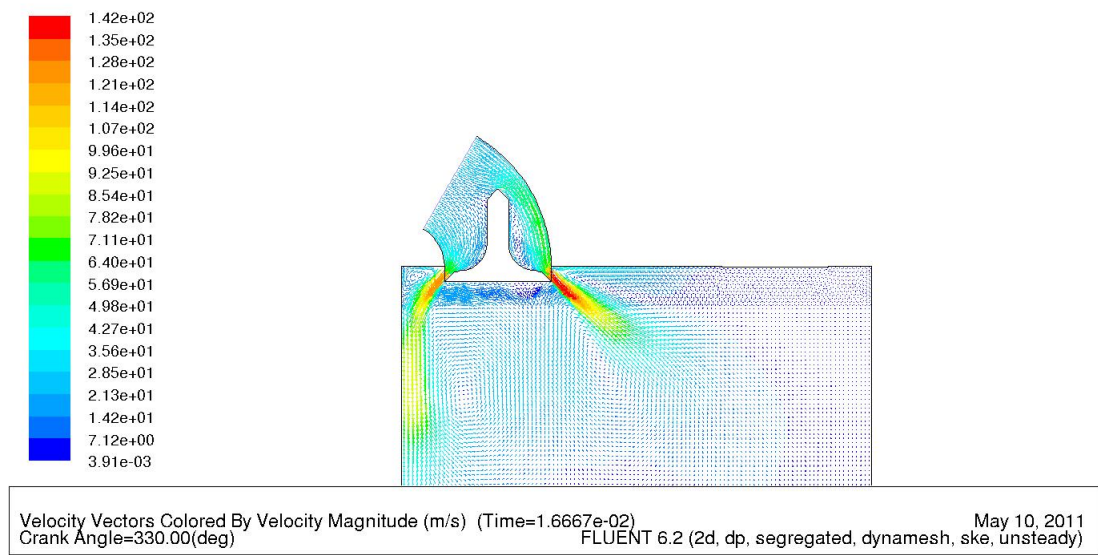


Figure 5.9: Vector plot of velocity at 150 crank angle for case 1 with 2D simulation

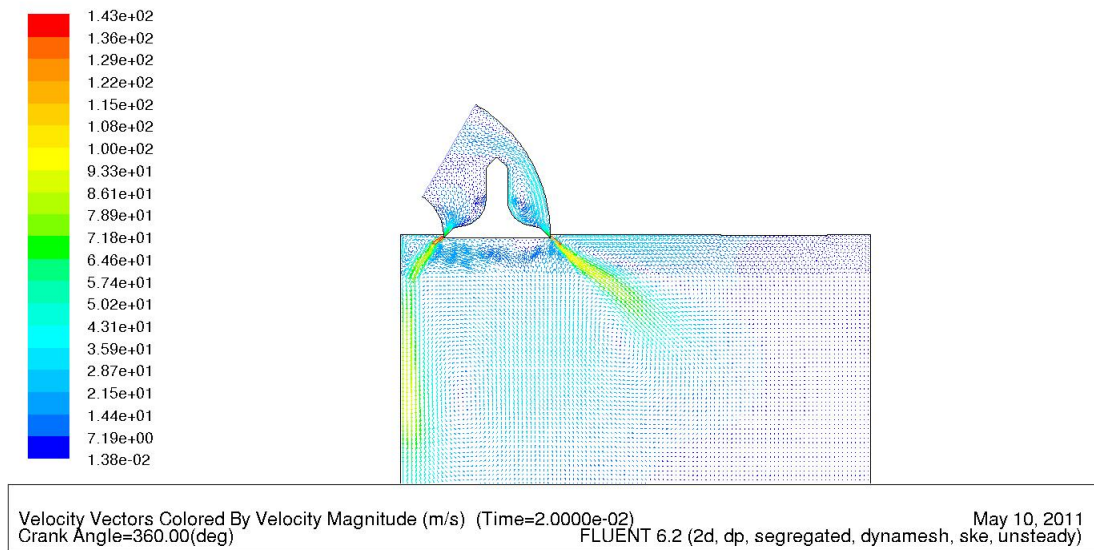


Figure 5.10: Vector plot of velocity at 180 crank angle for case 1 with 2D simulation

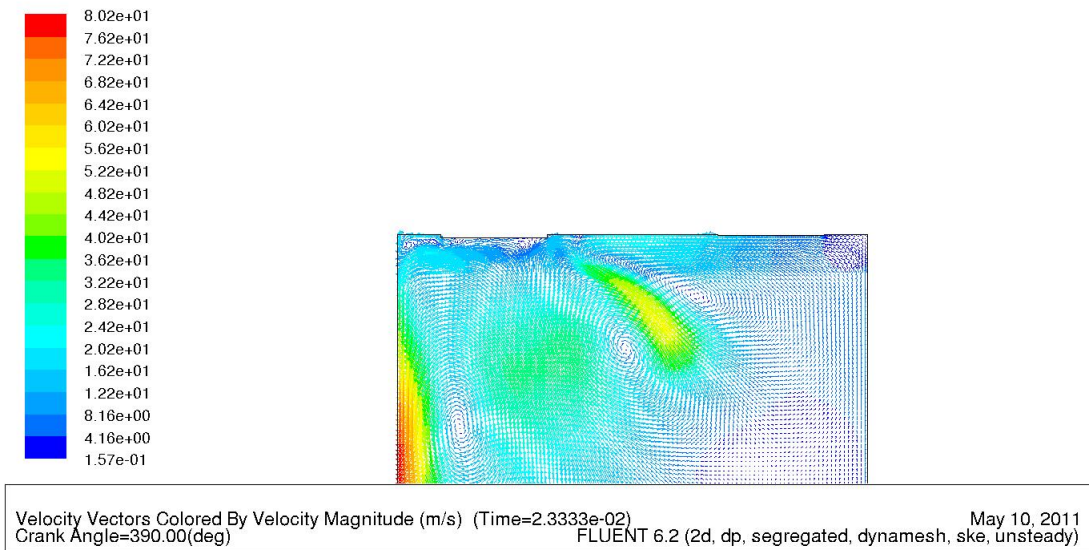


Figure 5.11: Vector plot of velocity at 210 crank angle for case 1 with 2D simulation

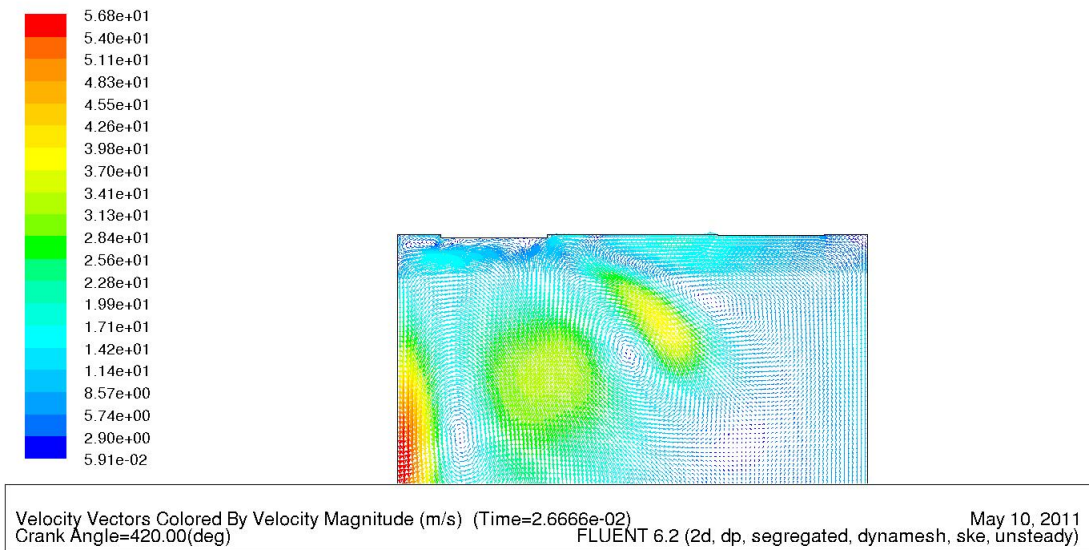


Figure 5.12: Vector plot of velocity at 240 crank angle for case 1 with 2D simulation

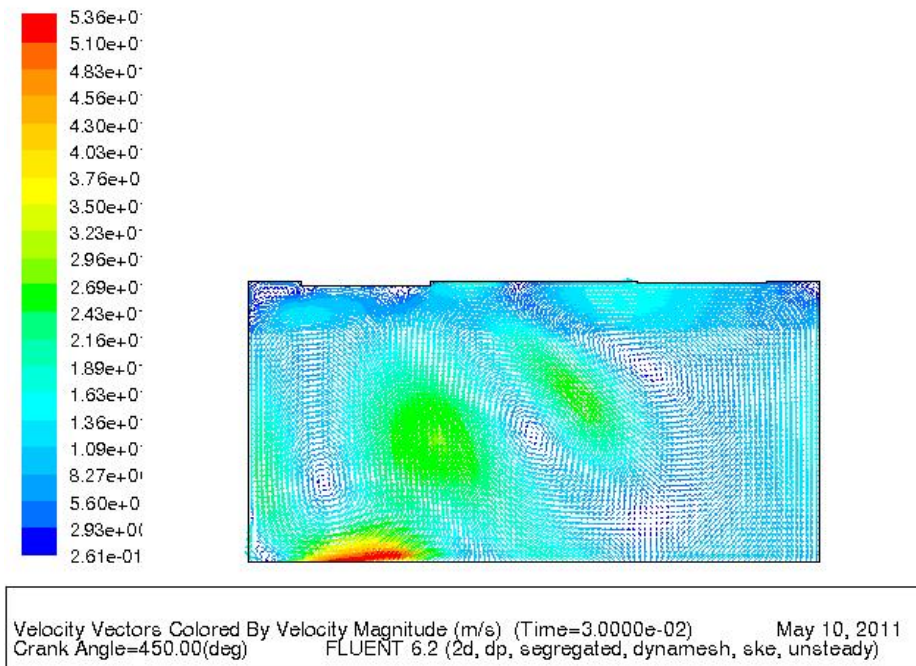


Figure 5.13: Vector plot of velocity at 270 crank angle for case 1 with 2D simulation

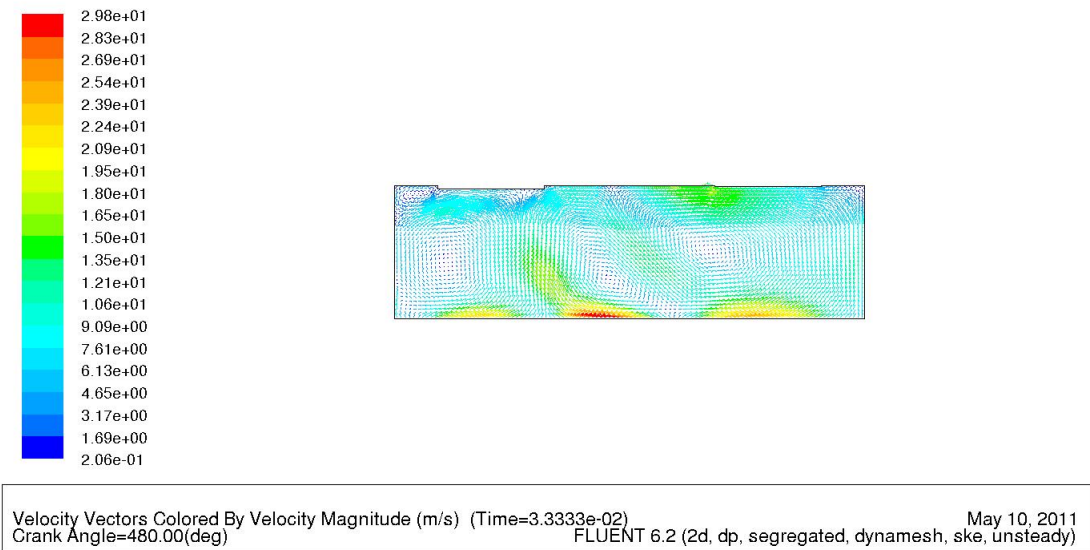


Figure 5.14: Vector plot of velocity at 300 crank angle for case 1 with 2D simulation

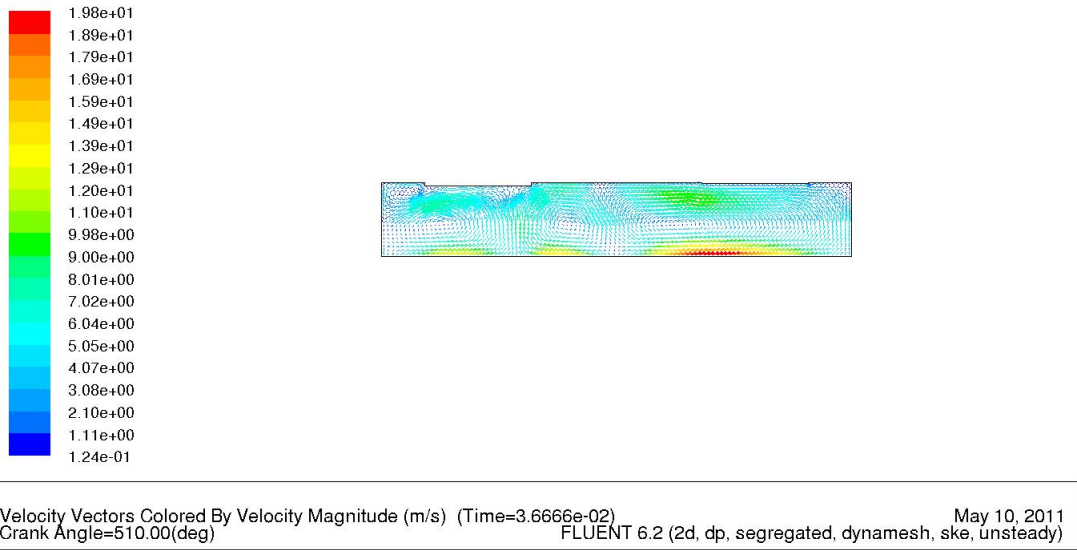


Figure 5.15: Vector plot of velocity at 330 crank angle for case 1 with 2D simulation

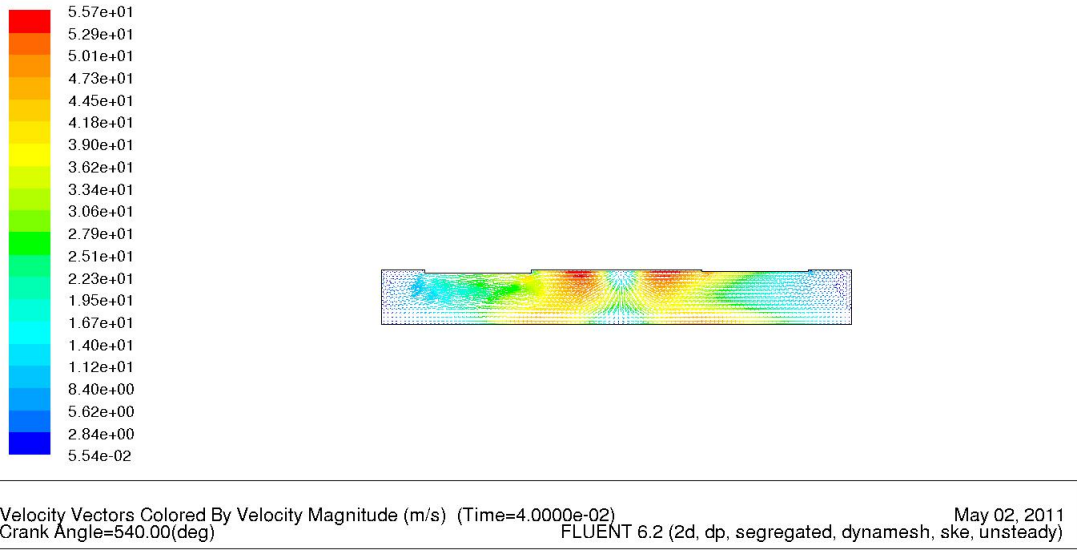


Figure 5.16: Vector plot of velocity at 360 crank angle for case 1 with 2D simulation

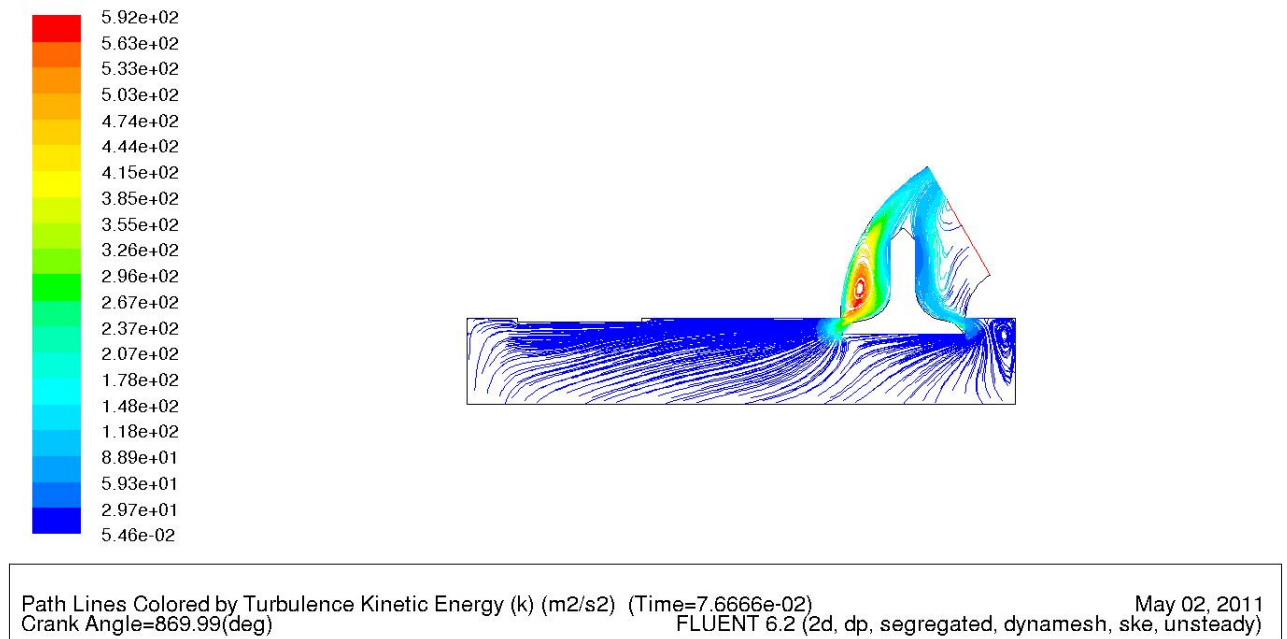
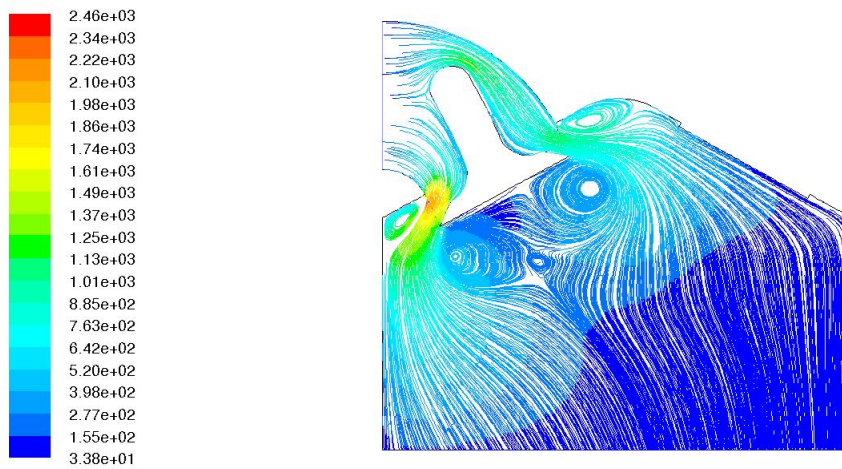


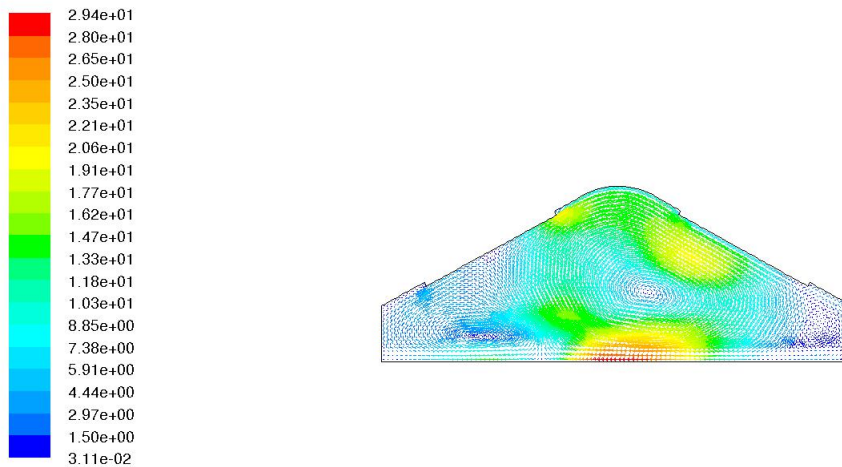
Figure 5.17: Pathlines of turbulence kinetic energy at 690 crank angle for case 9 with 2D simulation

Figure 5.18 to 5.21 shows vector plots of velocity and pathlines of turbulence kinetic energy at different crank angles. This shows the similar results as case 1 & 9. The turbulence is increase in suction stroke due to shear layer of high velocity jet entering the engine cylinder. Figure 5.18 shows that at 90 crank angles, wakes generated near intake valve due to high turbulence. This turbulence increases and goes high with high valve lift and piston speed. The turbulence will fall with the closer of intake valve. In compression process, turbulence decreases due to wall interactions. At the compression processes turbulence decays as shown in figure 5.19. Figure 5.21, shows the pathlines of turbulence at 690 crank angle for case 10, it shows that at the end of exhaust stroke sufficient turbulence is available in cylinder.



Path Lines Colored by Turbulence Intensity (%) (Time=9.9999e-03) May 02, 2011
 Crank Angle=270.00(deg) FLUENT 6.2 (2d, dp, segregated, dymesh, ske, unsteady)

Figure 5.18: Pathlines of turbulence kinetic energy at 90 crank angle for case 10 with 2D simulation



Velocity Vectors Colored By Velocity Magnitude (m/s) (Time=4.0000e-02) May 02, 2011
 Crank Angle=540.00(deg) FLUENT 6.2 (2d, dp, segregated, dymesh, ske, unsteady)

Figure 5.19: Vector plot of velocity at 360 crank angle for case 10 with 2D simulation

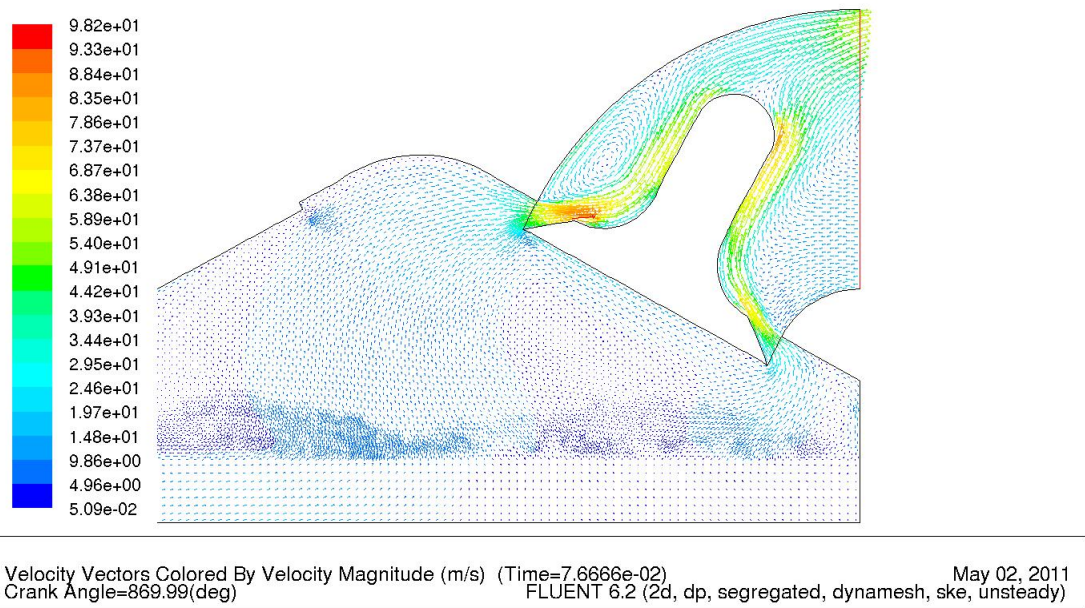


Figure 5.20: Vector plot of velocity at 690 crank angle for case 10 with 2D simulation

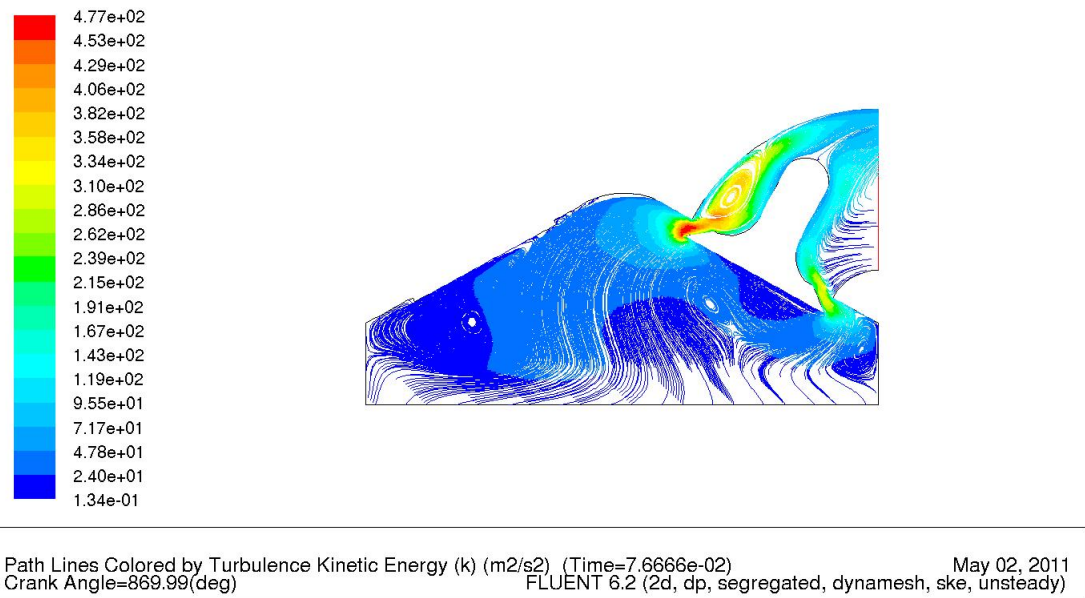


Figure 5.21: Pathlines of turbulence kinetic energy at 690 crank angle for case 10 with 2D simulation

5.4 Effect of engine speed

The variation of turbulent kinetic energy with engine speed for case 4 to 7 is shown in figures 5.22. As engine speed increases, turbulent kinetic energy increases this is due to increase in the velocity of jet entering into the cylinder and also due to increase of the fluid movement inside the cylinder. The peak for turbulent kinetic energy at each speed is approximately in the same range of crank angle and also the trend of turbulent kinetic energy is also same.

A variation of cylinder pressure with respect to crank angles is shown in figures 5.23. We can observe from figures that during compression stroke pressure increases and reaches to maximum value at 360 crank angles for which values are specified in figures. Then onwards during expansion stroke pressure once again reaches to atmospheric pressure due to increase in volume.

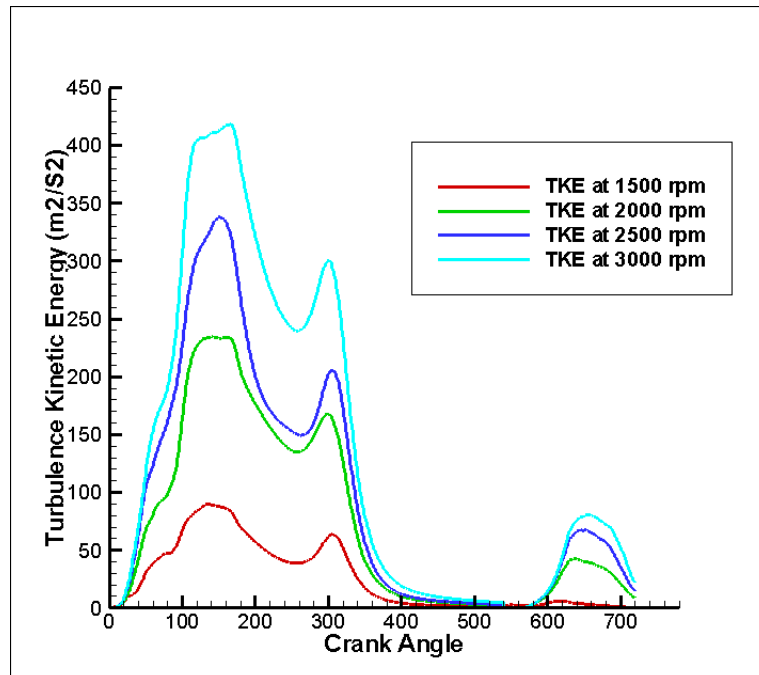


Figure 5.22: Volume average turbulent kinetic energy versus crank angle for various engine speeds for cases 4 to 7 with 2D simulations.

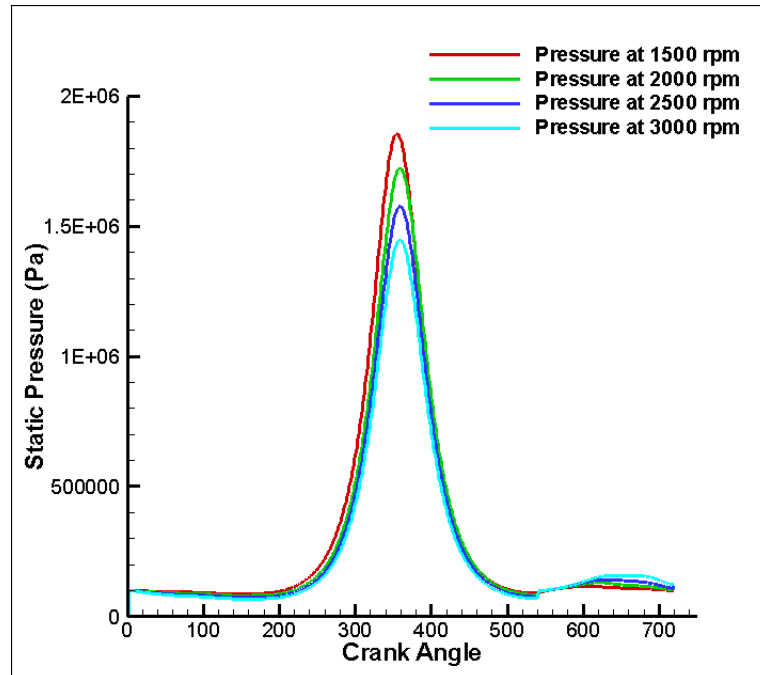


Figure 5.23: Volume average static pressure versus crank angle for various engine speeds for cases 4 to 7 with 2D simulations.

5.5 Premixed combustion model and spark ignition model analysis

Figure 5.24 and 5.26 shows the relation between volume average static temperature and crank angles for case 8 and 10. In case 8, the simulation of the engine process was done with premixed combustion model. The premixed combustion model with non-adiabatic condition has been taken in account. The fuel used is Methane (CH_4). To initiate the ignition of fuel and air mixture, the spark ignition model was used. The spark model with time varying spark radius was used. For methane-air mixture, a few millijoules of energy is enough to initiate the ignition under atmospheric condition but, in this simulation the very high energy of 120 joule is applied to achieve the ignition. The reason behind this concept is that in real practice, the only a small fraction of the energy is actually delivered to the air - fuel mixture and a lot of the energy is lost to heating the electrodes. For case 8, the spark duration

was kept as 2 milli seconds based on literature survey. The laminar flame speed was defined as 0.3 m/s. The spark model parameters are tabulated below:

Table 5.5: Spark model parameters for case 8

| Model | Time varaying spark radius |
|------------------|----------------------------|
| Shape | circle |
| Initial radius | 1 mm |
| Final radius | 5 mm |
| Spark Initiation | 360° CA |
| Spark energy | 120 Joul/ Second |
| Spark duration | 2 milli second |

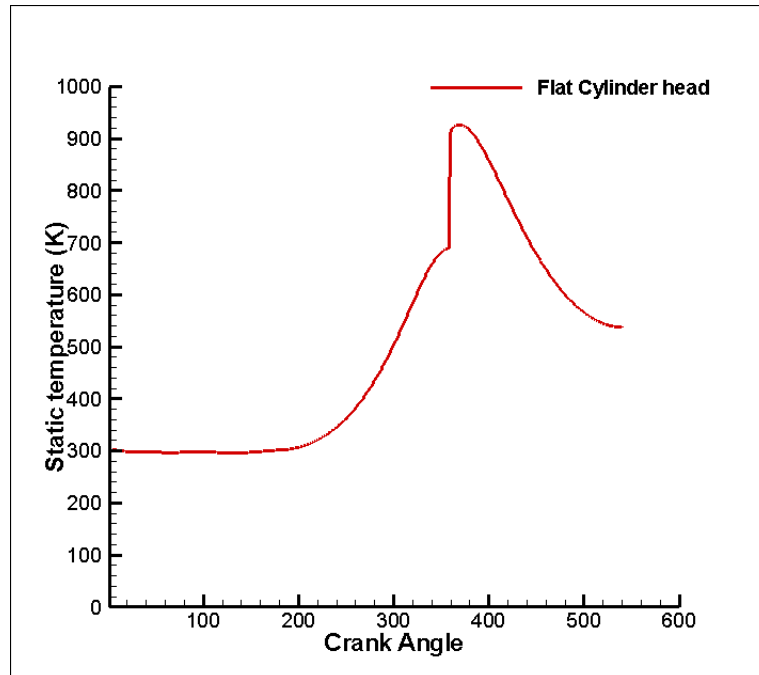


Figure 5.24: Volume average static temperature versus crank angle for cases 8

As shown in figure 5.24 , the temperature remains nearly constant to value of 300 K in intake process . In the compression stroke the temperature start increasing due compression of the air fuel mixture and the inward motion of piston . At the end of compression process the temperature reaches upto 686 K. The spark initiated at

the end of compression process, i.e. the sudden increase in temperature is achieved. As shown in figure 5.25, the temperature is about 2311 K at 360° crank angle or we can say at the end of compression process. The volume averaged temperature of the cylinder was about 940 K at 360° crank angle. In expansion process, the burning of air-fuel mixture takes place and the mixture was fully burnt during 37° crank angle rotation as shown in figure 5.28. After the burning of the mixture, the burnt gas remains in the cylinder and the volume averaged static temperature reaches to 550 K at the end of expansion process.

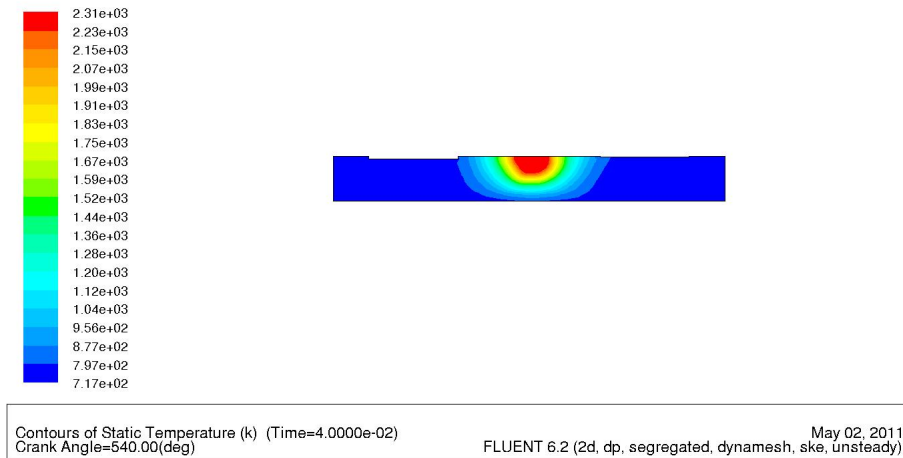


Figure 5.25: Contours of static temperature at 360 crank angle for case 8

Table 5.6: Spark model parameters for case 10

| Model | Time varying spark radius |
|------------------|---------------------------|
| Shape | circle |
| Initial radius | 1 mm |
| Final radius | 5 mm |
| Spark Initiation | 345° CA |
| Spark energy | 100 Joul/ Second |
| Spark duration | 3E-06 seconds |

Similarly, figure 5.26, shows the relation between volume averaged static temperature and crank angle for case 10. The premixed combustion model with time varying

spark model was applied for simulation of case 10. The spark plug locates at the midpoint of the hemispherical cylinder head. The spark parameters for case 10 are given in table 5.6.

As shown in figure 5.26, the temperature inside the cylinder remains nearly constant to the value of 300 K in intake stroke. After intake stroke, the temperature start increasng in compression process due to the air - fuel mixture get compress because of inward motion of the piston . At the end of compression stroke the volume average static temperature of the cylinder reach to 546 K. The spark intiate 15°crank angle before the end of compression stroke and the temperature at the time of spark was near about 1723 K. As shown in figure 5.27, the highest temperatute zone is near the hemispherical cylinder head and the static temperature at 360°crank angle was 1550 K. In expansion process, the volume average static temperature of the cylinder decreases and reach to 521 K at the end of expansion stroke. In the expansion stroke, the air - fuel mixture burning take place due to the higher temperature spark which propagates the flame karnel inside the cylinder and this cause the burning of whole air fuel mixture inside the cylinder.

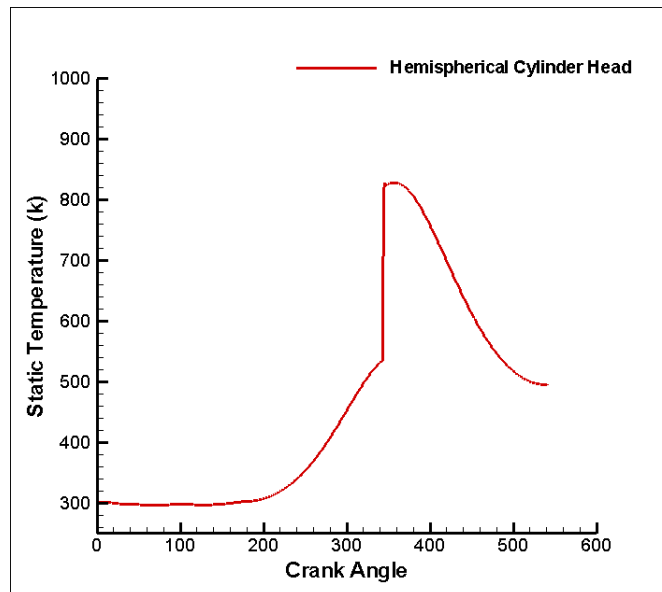


Figure 5.26: Volume average static temperature versus crank angle for cases 10

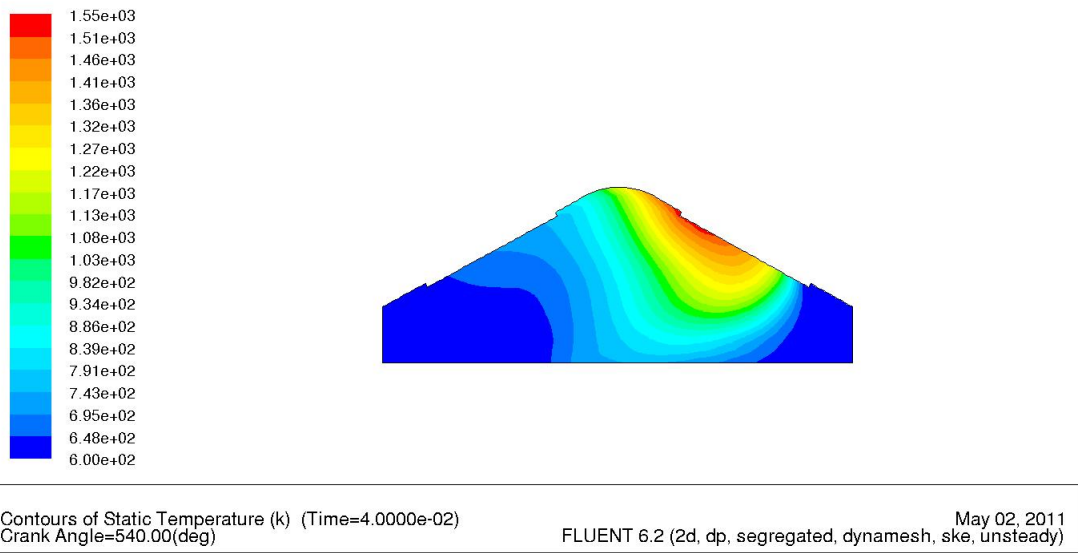


Figure 5.27: Contours of static temperature at 360 crank angle for case 10

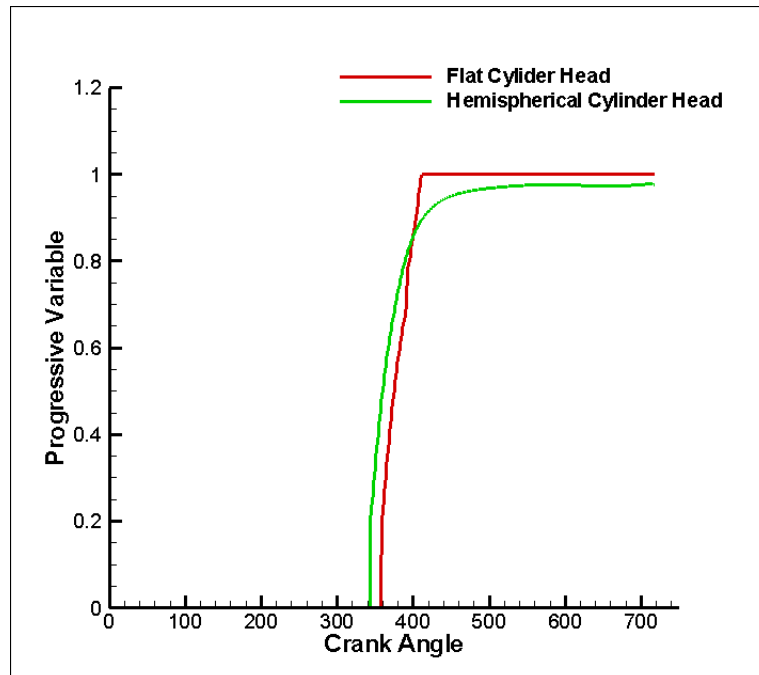


Figure 5.28: Volume average progressive variable versus crank angle for cases 8 & 10

Figure 5.28 shows the variation in progress variable at different crank angles for case 8 and 10. At the start of simulation, the value of progress variable is defined as zero i.e. $c = 0$, because value of progress variable is zero when the mixture is unburnt and unity when burnt. As shown in figure 5.28, the spark initiated at 360° crank angle for case 8 and at 345° crank angle for case 10. It shows that for case 8, the process of combustion was completed within the 37° crank angle after compression stroke and the unburnt mixture of air - fuel is fully burnt. At 397° crank angle, the value of progress variable reaches the 0.98, that shows that the mixture is fully burnt. The value of progress variable remains constant for next degrees of crank angle.

Similarly, for case 10, the spark initiated at 345° crank angles and the value of progress variable was defined zero. In this case, the process of combustion is continues more then 60° crank angles after the compression stroke. It may be happen that, the spark energy defined which was 100 joul may not be sufficient to increse the desirable rate of the combustion. Figure 5.28 shows that after 430° crank angle, the mixture is fully burnt and the progress variable attains the value of 0.95 at remaining crank angles.

Chapter 6

Conclusion and Scope of Future work

6.1 Conclusion

Examination of the computed cases results that initially turbulence is higher in the starting of suction stroke. In suction process the high turbulence is set in due to the shear layer in the high velocity jet entering the engine cylinder. The turbulence fluctuation increase and approximately go with the high piston speed and valve lift. There will be fall in turbulence with the closure of inlet valve. During the compression process, turbulence suddenly decreases due to wall interactions. At the end of compression process the turbulence will decays and this is desirable for better combustion because the spark initiates at the end of compression stroke. If at this instant, the higher turbulence can decay the process of spark initiation which is not desirable. High turbulence during suction & compression also helps for better mixing of air fuel mixture. Further the turbulence increase during exhaust process because at the end of compression process due to fluid movement in opposite direction, shear is generated which will give rise to turbulence. After this the turbulence will further decreases at the closer of exhaust valve. Results shows that turbulent kinetic energy is highly sensitive to change is engine speed and . The analysis with premixed combustion shows that the combustion completed within the 37°crank angles after compression stroke for flat cylinder head geometry and the temperature rises to the sufficient limit .

6.2 Scope for future work

The present work deals with the simulation of an engine in motored case and with premixed combustion in 2D for flat piston and flat & hemispherical cylinder head. In future, the simulation can be done with changing the different cylinder head and engine performance variables. The 3D simulation of engine can also be done.

Bibliography

- [1] Heywood J.B. (1998) "Internal Combustion Engine Fundamentals", McGraw-Hill, New York. 2, 3
- [2] J. E. Bardina, P. G. Huang, T. J. Coakley (1997), "Turbulence Modeling Validation, Testing, and Development", NASA Technical Memorandum 110446.
5
- [3] Veynante D., Vervisch L.(2002), "Turbulent combustion modeling", Progress in energy and combustion science 28 (2002) 193-266. 8
- [4] Poinso T., Veynante D.(2005), "Theoretical and numerical combustion", R.T.Edward Inc., Philadelphia. 9
- [5] Z. Barbouchi and J. Bessrouf (2009), "Turbulence study in the internal combustion engine", Journal of Engineering and Technology Research Vol.1 (9), pp. 194-202. 10
- [6] R.F. Huang, H.S. Yang, C.-N. Yeh (2008), "In-cylinder flows of a motored four-stroke engine with flat-crown and slightly concave-crown pistons", Experimental Thermal and Fluid Science 32 (2008) 1156-1167. 11, 12
- [7] Kihyung Lee, Choongsik Bae, Keryong Kang (2007), "The effects of tumble and swirl flows on flame propagation in a four-valve S.I. engine", Applied Thermal Engineering 27 (2007) 2122-2130. 12

- [8] R.F. Huang, C.W. Huang, S.B. Chang, H.S. Yang, T.W. Lin, W.Y. Hsu(2007), “Topological flow evolutions in cylinder of a motored engine during intake and compression strokes”, *Journal of Fluids and Structures* 20 (2005) 105127. 13
- [9] Nureddin Dinler, and Nuri Yucel(2007) , “Numerical Simulation of Flow and Combustion in an Axisymmetric Internal Combustion Engine”, *Engineering and Technology* 36 2007. 14
- [10] Versteeg H.K., Malalasekera W.(1995), “An introduction to computational fluid dynamics - The finite volume method”, John wileys & sons, NewYork. 18, 19
- [11] Anderson J.D.(1995), “Computational fluid dynamics - the basics with applications”, McGraw-Hill, New York. x, 19, 24, 25, 26
- [12] FLUENT user guides, 2005 (Volume 1, 2, 3) 32, 33, 34, 35
- [13] M.H. Shojaeefard and A.R. Noorpoor(2008), Flow Simulation in Engine Cylinder with Spring Mesh, *American Journal of Applied Sciences* 5 (10): 1336-1343, 2008.